LOS ALAMOS SCIENTIFIC LABORATORY
OF THE UNIVERSITY OF CALIFORNIA ○ LOS ALAMOS   NEW MEXICO

① Hydrodynamics
② Gasdynamics
③ Blast
④ Mathematics

THE PARTICLE-IN-CELL METHOD

FOR HYDRODYNAMIC CALCULATIONS

LEGAL NOTICE

LOS ALAMOS SCIENTIFIC LABORATORY
OF THE UNIVERSITY OF CALIFORNIA   LOS ALAMOS   NEW MEXICO

THE PARTICLE-IN-CELL METHOD
FOR HYDRODYNAMIC CALCULATIONS*

by

Martha W. Evans
Francis H. Harlow

Appendix II

by

Eleazer Bromberg

Machine Calculations

by

Eleazer Bromberg   Chester S. Kazek, Jr.
Martha W. Evans   Helen Korell
Ruth M. Gilmer   Chalkley Murray
David E. Harris, Jr.   George H. Pimbley

ABSTRACT

A method is presented for solving hydrodynamic prob-
lems involving large distortions and compressions of the
fluid in several space dimensions. The calculation procedure
introduces finite difference approximations to the differ-
ential equations; the solution in practice is carried out by
means of high-speed electronic computers. The paper dis-
cusses a number of characteristics of the method and il-
lustrates these by presenting results of representative calcu-
lations.

CONTENTS

INTRODUCTION

Realistic studies of the complicated dynamics of compressible fluids are being made possible by recent development of large high-speed computing machines. Methods are well known for treating problems dependent upon one space coordinate only ("1-D" problems). For those dependent upon two or more space coordinates ("2-D" problems, etc.), several methods of treatment have been used with success in restricted classes of problems. Features of these, pertinent to this report, are discussed in Appendix I.

It is our purpose here to present and discuss a method* for solving 2- and 3-D problems which, in a number of preliminary studies, has appeared successful for solving problems involving large distortions in systems with several fluids.

We acknowledge with pleasure the stimulation, encouragement, and valuable criticisms that have come from numerous discussions with Garrett Birkhoff, Eleazer Bromberg, Rolf Landshoff, Robert D. Richtmyer, A. H. Taub, and Stanislaw Ulam.

---

*F. H. Harlow, J. Assoc. Comp. Mach., $\underline{4}$, 137 (April, 1957).

Chapter I

THE METHOD

A. General Description

The calculation procedure which is here described combines features of several of those discussed in Appendix I. The space occupied by the fluid is divided into a network of fixed cells through which the fluid moves. The fluid within these cells is represented by particles, each of which carries a fixed mass of fluid. Their coordinates vary with time as they move through the mesh of cells. Thus we have a Lagrangian coordinate system superimposed upon an Eulerian one.

For convenience, we refer to the procedure to be described, as the "Particle-in-Cell Method," abbreviated "PIC."

B. PIC in One Space Dimension

Characteristics of method are most easily demonstrated in application to 1-D problems, but PIC attempts competition with other methods only for 2- and 3-D calculations.

Assume only one material to be present in a closed one-dimensional box. The system of equations which we wish to solve, subject to initial and boundary conditions, is:

$$\frac{\partial \rho}{\partial t} + \frac{\partial \rho u}{\partial x} = 0 \qquad \text{(1)}$$

$$\rho \frac{\partial u}{\partial t} + \rho u \frac{\partial u}{\partial x} = -\frac{\partial p}{\partial x} \qquad \text{(2)}$$

transport term

$$\rho \, \frac{\partial E}{\partial t} + \rho u \, \frac{\partial E}{\partial x} = - \, \frac{\partial pu}{\partial x} \qquad (3)$$

$$p = f(\rho, I) \qquad (4)$$

where

ρ = density

u = velocity

p = pressure

I = specific internal energy

E = specific energy = $I + \frac{1}{2}u^2$

Relation (4) represents the equation of state of the fluid. The absence of heat conduction, viscosity, or other dissipative mechanism means that the true solution may possess or develop mathematical singularities. This possibility is ignored at first.

The box is divided into cells of equal length, s, labeled with index c (c = 1, 2, . . ., L). Into this, particles of equal mass, m, are arranged with number N_c in each cell in such a manner that the initial density profile is represented.

The calculation to advance the configuration in time proceeds in steps or cycles, each of which calculates the desired quantities for time $t + \delta t$ in terms of those at time t (an "explicit" time advancement procedure). This introduces nothing novel, however, as long as δt is small enough to satisfy criteria discussed later. Our principal attention is devoted to the spatial features of the calculation.

A division of each cycle of calculation into three phases is convenient. In Phase I the Eulerian field functions are changed, neglecting transport due to fluid motion. Phase II accomplishes the motion of the particles to their new positions. The transport corrections are accomplished in Phase III. Generally, a Phase IV is also added in which various diagnostic functionals of motion are calculated for that cycle.

Phase I

Each cell has density, $\rho_c \equiv \frac{N_c m}{s}$, specific internal energy, I_c, velocity, u_c, and pressure, $p_c = f(\rho_c, I_c)$. All of these are the values at the cell centers, but are assumed to hold for a particle anywhere in a cell. Dropping the transport term in Equation (2), and transforming it to our finite difference form,

$$\frac{N_c m}{s} \frac{\partial u_c}{\partial t} = -\frac{1}{2s}\left(p_{c+1} - p_{c-1}\right) \tag{5}$$

A similar treatment of Equation (3) leads to

$$\frac{N_c m}{s}\left(\frac{\partial I_c}{\partial t} + u_c \frac{\partial u_c}{\partial t}\right) = -\frac{1}{2s}\left[(pu)_{c+1} - (pu)_{c-1}\right] \tag{6}$$

These equations can be combined and rearranged:

$$\frac{\partial u_c}{\partial t} = \frac{1}{2N_c m}\left(p_{c-1} - p_{c+1}\right) \tag{7}$$

$$\frac{\partial I_c}{\partial t} = \frac{1}{2N_c m}\left[p_{c-1}\left(u_{c-1} - u_c\right) - p_{c+1}\left(u_{c+1} - u_c\right)\right] \tag{8}$$

When the intitial and boundary conditions have been specified, then the quantities on the right sides are all known at time t and the time derivatives can be calculated.

Let $t = n\delta t$. Then

$$\tilde{u}_c = u_c^n + \delta t \left(\frac{\partial u_c}{\partial t}\right)^n$$

$$\tilde{I}_c = I_c^n + \delta t \left(\frac{\partial I_c}{\partial t}\right)^n \tag{9}$$

where the superscript represents the time cycle number and the tilde symbolizes the fact that these advanced time quantities are yet to be corrected by the transport terms.

An alternate form for the energy equation can be obtained. If in Equation (6) we make the change,

$$u_c \frac{\partial u_c}{\partial t} \rightarrow \frac{1}{2}\frac{\partial u_c^2}{\partial t} \rightarrow \frac{1}{2\delta t}\left[(\tilde{u}_c)^2 - (u_c^n)^2\right]$$

and shift the result to the right side of the equation, we would obtain, in

- 10 -

place of Equation (8),

$$\frac{\partial I_c}{\partial t} = -\frac{1}{2\delta t}\left[(\tilde{u}_c)^2 - (u_c^n)^2\right] + \frac{1}{2N_c m}\left(p_{c-1} u_{c-1} - p_{c+1} u_{c+1}\right) \tag{8'}$$

All the calculations reported in this paper used the energy equation in the form of Equation (8). Boundary conditions, the same for either form, are discussed later in connection with questions of conservation.

Phase II

The particles are moved. Although each particle in cell c now carries momentum $m\tilde{u}_c$, it is moved according to a "velocity-weighting" procedure. The effective moving velocity is obtained by a <u>linear interpolation</u> according to the position of the particle between the centers of two cells, using the velocity at each center. Labeling the particles with j, we write

$$x_j^{n+1} = x_j^n + u_{eff}\,\delta t \tag{10}$$

The value of u_{eff} is computed from values of u_c^n.

Phase III

The transport corrections are accomplished in this phase. For those cells which change particle number in Phase II, additional calculations are required. The procedure is called "repartitioning." Otherwise, the tilde values of Phase I become final, and the cycle is complete.

Suppose that the only boundary crossing involves a particle going from cell c - 1 to cell c. For cell c - 1 the only change recorded is $N_{c-1}^{n+1} = N_{c-1}^n - 1$. Correspondingly N_c is increased by 1. *i.e* $N_c^{n+1} = N_c^n + 1$

Furthermore, the velocity of cell c becomes

$$u_c^{n+1} = \frac{N_c^n \tilde{u}_c + \tilde{u}_{c-1}}{N_c^n + 1} \tag{11}$$

this means for phase III (not whole cycle)

so that the <u>momentum of the system is unchanged.</u> The kinetic energy of the system drops, however, the change being

$$\delta KE = KE^{n+1} - KE^n = \frac{1}{2}m\left(N_c^n+1\right)\left[\frac{N_c^n\tilde{u}_c + \tilde{u}_{c-1}}{N_c^n+1}\right]^2 - \left[\frac{1}{2}mN_c^n(\tilde{u}_c)^2 + \frac{1}{2}m(\tilde{u}_{c-1})^2\right] =$$

$$\delta KE = -\frac{m}{2}\left(\frac{N_c^n}{N_c^n+1}\right)\left(\tilde{u}_{c-1} - \tilde{u}_c\right)^2 \tag{12}$$

The specific internal energy is modified by the transport effect and, to conserve total energy, is increased by the amount of loss in specific kinetic energy.

$$I_c^{n+1} = \frac{N_c^n\tilde{I}_c + \tilde{I}_{c-1}}{N_c^n + 1} + \frac{|\delta KE|}{m\left(N_c^n + 1\right)} \tag{13}$$

When a cell has both outgoing and incoming particles, the latter repartition only with those which remain after the outgoing ones have left. Otherwise, an unreal transport of energy is added.

C. Discussion of 1-D PIC Method

1. Energy and Momentum. The difference equations of Phase I can be obtained in several ways and written in several forms. A discussion is given in Appendix II. In particular, Equation (8) is more complicated than the analogous equation one would obtain by starting with the differential equation

$$\rho\frac{\partial I}{\partial t} + \rho u\frac{\partial I}{\partial x} = -p\frac{\partial u}{\partial x} \tag{14}$$

instead of Equation (3). The reasons for our choice are brought out by looking at the problem of over-all conservation of energy in Phase I.

The total energy of the system at time t is

$$E^n = \sum_c N_c m\left[I_c^n + \frac{1}{2}\left(u_c^n\right)^2\right] \tag{15}$$

Likewise, by the end of Phase I it has changed to

$$\tilde{E} = \sum_c N_c m\left[\tilde{I}_c + \frac{1}{2}\left(\tilde{u}_c\right)^2\right] \tag{16}$$

- 12 -

the total change being

$$\widetilde{E} - E^n = \delta E = \sum_c N_c m \left[\widetilde{I}_c - I^n_c + u^n_c \left(\widetilde{u}_c - u^n_c \right) \right]$$

(17)

$$+ \frac{1}{2} \sum_c N_c m \left(\widetilde{u}_c - u^n_c \right)^2$$

Define:

$$\delta D \equiv \frac{1}{2} \sum_c N_c m \left(\widetilde{u}_c - u^n_c \right)^2$$

(18)

These, with Equations (6) and (9), become

$$\delta E = \delta D + \frac{\delta t}{2} \sum_{c=1}^{L} \left[(pu)_{c-1} - (pu)_{c+1} \right]$$

(19)

$$\delta D = \frac{(\delta t)^2}{2} \sum_c N_c m \left(\frac{\partial u_c}{\partial t} \right)^2$$

(20)

In terms of two fictitious cells beyond the system ($c = 0$ and $c = L + 1$) Equation (19) can be written

$$\delta E = \delta D + \delta t \left[\frac{(pu)_0 + (pu)_1}{2} - \frac{(pu)_L + (pu)_{L+1}}{2} \right]$$

(21)

The cancellation of terms in pairs, exploited here, would not have occurred had we started from Equation (14) in the difference equation derivations.

The important quantity, δD, represents the only discrepancy in energy of the entire cycle calculation, since Phases II and III conserve energy rigorously. This nonconservation would not have appeared had Equation (8') been used for internal energy calculations. Since $\delta D \geqslant 0$, the total observed energy rises monotonically above that which theoretically is present. This fact can, indeed, be generalized to include multidimensional applications of PIC with various boundary conditions, conservative or not. δD is an important Phase IV functional to be calculated since its disagreement, beyond

- 13 -

$$\frac{\delta D_c}{KE_c} = \frac{\frac{\delta t^2}{2} N_c m \left(\frac{\partial u_c}{\partial t}\right)^2}{\frac{1}{2} N_c m (u_c)^2} = \left[\frac{\frac{\partial u_c}{\partial t} \delta t}{u_c}\right]^2$$

machine round-off, with the observed discrepancy is a powerful indicator of almost any error, mechanical or human.

Knowledge of δD is of value also for the purpose of limiting the size of δt. Since δD is proportional to $(\delta t)^2$, its cumulative effect over a fixed time interval is proportional to δt. The time interval should be small enough so that the over-all discrepancy through a problem is insignificant. Effectively, this means $\dot{u}\delta t/u \ll 1$ is required, since the ratio of the specific discrepancy to the specific kinetic energy is just $(\dot{u}\delta t/u)^2$. Notice that when the velocity starts from zero, then in the first cycle, all the kinetic energy that is produced goes into discrepancy!

Tests have shown that when δt is small enough to produce negligible values of δD, then all inaccuracies due to time differencing are negligible. In this case, calculations using either Equation (8) or (8') are equivalent, and the more convenient form may be employed.

Equation (21) shows how the boundary conditions are to be chosen for conservation of energy: the average value of pu (the energy flux) must vanish at each boundary. With $p_0 \equiv p_1$ and $u_0 \equiv -u_1$ the boundary is reflective. No other arrangement is reasonable in this case.

Since Phases II and III rigorously conserve momentum, we may derive from Equations (5) and (9) that the change in momentum, δM, in a cycle is given exactly by

$$\delta M = \delta t \left[\frac{p_0 + p_1}{2} - \frac{p_L + p_{L+1}}{2}\right]$$

$$\delta M = \tilde{M} - M^n = \sum_c N_c m \tilde{u}_c - \sum_c N_c m u_c^n = \sum_c N_c m (\tilde{u}_c - u_c^n) = \sum_c N_c m \, \delta t \left(\frac{\partial u_c}{\partial t}\right)^n$$

$$= \sum_{c=1} N_c m \, \delta t \left(-\frac{1}{N_c m}\right)(p_{c+1} - p_{c-1}) = \frac{\delta t}{2} \sum_c (p_{c-1} - p_{c+1})$$

(22)

Comparison of the observed change with this theoretical change in each cycle makes another good calculation check, since the agreement should be to within machine round-off errors.

A complication arises in the Phase I calculations wherever a cell becomes empty. Equations (7) and (8) cannot be used for such cells; indeed, one need not bother to calculate in them at all in Phase I. But unless special care is devoted to the adjacent cells, the system will suffer significant energy discrepancies. A reasonable procedure which is consistent with the conservation laws is as follows. Let cell c be empty. When calculating in cell c − 1, consider that cell c has $p_c = -p_{c-1}$, $u_c = +u_{c-1}$. When calculating in cell c + 1, consider that cell c has $p_c = -p_{c+1}$, $u_c = +u_{c+1}$. Similar procedures hold in the applications of PIC to 2-D problems.

2. Diffusion and Accuracy. Certain other important characteristics of PIC are shown by the following analysis.

We define ρ_{c+a}^n as the average mass per unit distance at time $n\delta t$ and

position $(c + a)s$. Then to lowest order in the cell size and zero order in δt, the result of all three phases of the calculation can be summarized by the equations

$$\frac{\partial u_c}{\partial t} = \frac{1}{2\rho_c s} \left(p_{c-1} - p_{c+1} \right) + \rho_{c-\frac{1}{2}} u_{c-\frac{1}{2}} \left(\frac{u_{c-1} - u_c}{\rho_c s} \right) \tag{23}$$

$$\frac{\partial I_c}{\partial t} = \frac{1}{2\rho_c s} \left[p_{c-1} \left(u_{c-1} - u_c \right) - p_{c+1} \left(u_{c+1} - u_c \right) \right]$$

$$+ \rho_{c-\frac{1}{2}} u_{c-\frac{1}{2}} \left(\frac{I_{c-1} - I_c}{\rho_c s} \right) + \frac{1}{2\rho_c s} \rho_{c-\frac{1}{2}} u_{c-\frac{1}{2}} \left(u_{c-1} - u_c \right)^2 \tag{24}$$

$$s \frac{\partial \rho_c}{\partial t} = \rho_{c-\frac{1}{2}} u_{c-\frac{1}{2}} - \rho_{c+\frac{1}{2}} u_{c+\frac{1}{2}} \tag{25}$$

where it is assumed that all the velocities are positive in the direction of increasing cell index. Also,

$$u_{c\pm\frac{1}{2}} \equiv \frac{u_c + u_{c\pm 1}}{2} \tag{26}$$

Equation (25) is clearly in conservation form. The other two can also be put into the completely conservative forms

$$\frac{\partial \rho_c u_c}{\partial t} = \frac{1}{2s} \left(p_{c-1} - p_{c+1} \right) + \frac{1}{s} \left(u_{c-1} \rho_{c-\frac{1}{2}} u_{c-\frac{1}{2}} - u_c \rho_{c+\frac{1}{2}} u_{c+\frac{1}{2}} \right)$$

$$\frac{\partial \rho_c E_c}{\partial t} = \frac{1}{2s} \left[(pu)_{c-1} - (pu)_{c+1} \right] + \frac{1}{s} \left(E_{c-1} \rho_{c-\frac{1}{2}} u_{c-\frac{1}{2}} - E_c \rho_{c+\frac{1}{2}} u_{c+\frac{1}{2}} \right)$$

by some simple algebraic manipulations.

Now expand, by Taylor series, the right side of Equation (23) about the center of cell c. Dropping the index we get

$$\rho \frac{\partial u}{\partial t} = -\frac{\partial p}{\partial x} - \rho u \frac{\partial u}{\partial x} + \frac{\partial}{\partial x} \left(\lambda' \frac{\partial u}{\partial x} \right) + O(s^2) \tag{27}$$

Similarly from Equation (24),

$$\rho \frac{\partial I}{\partial t} = -p \frac{\partial u}{\partial x} - \rho u \frac{\partial I}{\partial x} + \frac{\partial}{\partial x}\left(\lambda' \frac{\partial I}{\partial x}\right) + \lambda'\left(\frac{\partial u}{\partial x}\right)^2 + O(s^2) \qquad (28)$$

and from Equation (25)

$$\frac{\partial \rho}{\partial t} = -\frac{\partial \rho u}{\partial x} + O(s^2) \qquad (29)$$

where

$$\lambda' \equiv \frac{1}{2}\rho us \qquad (30)$$

From these results, many of the most striking characteristics of PIC can be learned. Of particular interest is the fact that repartitioning does incorporate, to lowest order, the correct transport terms into the equations. The next order term in the momentum equation has exactly the form of a "true" viscosity term with coefficient of viscosity $\lambda' = \frac{1}{2}\rho us$. The corresponding term, $\lambda'(\partial u/\partial x)^2$, in the energy equation also has the proper form of a "true" viscosity effect.

The form of the one-dimensional effective viscosity λ' bears a striking resemblance to the "linear viscosity" introduced by Landshoff*:

$$\lambda'_L = \frac{1}{2}\rho cs$$

where c is the local sound speed. The resemblance to the classical artificial viscosity of von Neumann and Richtmyer** is less close, as theirs possesses a velocity gradient factor.

The λ' terms have several effects on the calculation. Most important, they symbolize the dissipation which is present in regions of rapid change, such as regions which would contain shocks in the true solution. They allow the calculation to reproduce correctly the macroscopic features of a shock without requiring special care concerning its microscopic features.

The λ' terms also symbolize inaccuracy in the calculations. But at the

---

* R. Landshoff, Los Alamos Scientific Laboratory Report LA-1930, "A Numerical Method for Treating Fluid Flow in the Presence of Shocks," Department of Commerce, Office of Technical Services, Washington 25, D.C. (1955).

**J. von Neumann and R. Richtmyer, J. Appl. Phys., 21, 232 (1950).

same time they suggest a cure, since the effect of the terms can be made cumulatively as small as desired by decreasing the cell size. Various specific criteria can be established of the following sort. Suppose that ρ and u are everywhere constant in space. Then the condition that the diffusion term be negligible compared with the transport term in the energy equation is that

$$\frac{s}{2} \ll \frac{\left(\frac{\partial I}{\partial x}\right)}{\left(\frac{\partial^2 I}{\partial x^2}\right)} \tag{31}$$

The right side is a measure of the distance over which the slope changes appreciably. By similar conditions applied to other field functions one may arrive at the general statement:

PIC will produce relative errors in the equations of motion which are roughly equal to the ratio of the cell size to the smallest physically significant dimension of the system.

There is some hope that this statement is pessimistic. Certainly some functionals of the motion will be more truly represented than others when the mesh is coarse. Examples of this are presented later.

One catastrophe that can occur in PIC calculations arises when the cell next to a left reflective boundary has an empty neighbor on its right. The energy Equation (8) for the cell becomes

$$\frac{\partial I}{\partial t} = -\frac{pu}{\rho s}$$

and the acceleration Equation (7) becomes

$$\frac{\partial u}{\partial t} = \frac{p}{\rho s}$$

If u and I (and thus p) are negative, then the cell is unstable since both $\partial I/\partial t$ and $\partial u/\partial t$ are negative. Starting from the moment of zero velocity, the time required for the temperature and velocity to reach $-\infty$ is $T_{-\infty} = \frac{\pi}{2}\sqrt{\frac{2s}{(\gamma-1)u_0}}$, where we have assumed a polytropic gas of exponent γ and an initial acceleration in the cell of $-\dot{u}_0$.

Equation (28) shows that negative temperatures can arise if the cell size is large enough. Suppose that I and p are both zero. Then $\partial I/\partial t$ can be negative if

$$-\rho u \frac{\partial I}{\partial x} + \frac{s}{2} \left[\frac{\partial}{\partial x} \left(\rho u \frac{\partial I}{\partial x} \right) + \rho u \left(\frac{\partial u}{\partial x} \right)^2 \right] < 0$$

With $u > 0$ and $\partial I/\partial x < 0$, this condition becomes

$$\frac{\partial}{\partial x} \left(\rho u \frac{\partial I}{\partial x} \right) < -\rho u \left[\left(\frac{\partial u}{\partial x} \right)^2 + \frac{2}{s} \left| \frac{\partial I}{\partial x} \right| \right]$$

in order to produce negative temperatures. As s becomes small there is reached a value, s_0, corresponding to a particular continuous configuration, such that for smaller s, $\partial I/\partial t$ is no longer negative. Physically, this corresponds to passing the point beyond which internal energy is transported into a cell faster than it can be converted to kinetic energy. If $\partial I/\partial x = 0$, then the requirement for $\partial I/\partial t < 0$ becomes, instead,

$$\frac{\partial^2 I}{\partial x^2} < - \left(\frac{\partial u}{\partial x} \right)^2$$

which means that I must be locally a maximum. Since, however, $I = 0$, we see that this situation does not arise.

A further condition (more stringent than necessary) is derived by setting $\partial u/\partial x = 0$. In that case we see that

$$s_0 = \frac{2\rho \left| \frac{\partial I}{\partial x} \right|}{\frac{\partial}{\partial x} \left(\rho \left| \frac{\partial I}{\partial x} \right| \right)}$$

which means that to avoid negative temperatures, s must be smaller than the distance over which $\rho |\partial I/\partial x|$ changes appreciably.

These ideas indicate some of the causes and cures for negative temperatures and the inaccuracies they symbolize. Peculiar equations of state and other fictitious situations can also cause negative temperatures.

The time interval, δt, between cycles has already been restricted by requiring the energy discrepancy of Equation (20) to be sufficiently small. It is also restricted by the condition $(c\delta t)/s < 1$ which is required for stability of the difference equations. Experience shows that even a slight violation of this condition leads to catastrophe. A further restriction is the requirement that $(u_{max}\delta t)/s < 1$, where u_{max} is the maximum fluid speed in the system. This mechanical restriction arises from the fact that no

allowance is made for a particle to travel more than a cell width in any one cycle. The following conditions probably make the last restriction even stricter: The success of PIC depends, clearly, upon there being a statistical averaging effect. It is reasonable to suppose that this will be enhanced if, during a certain elapsed problem time, the particles experience many different orientations relative to the mesh. This will occur if $(u_{max}\delta t)/s \ll 1$ so that many steps are required to move a particle across each cell.

The difficulties concerning statistical fluctuations and their proper averaging in PIC raise, perhaps, the most difficult question to discuss in desired generality. There are situations in which one would not expect averaging to proceed well. An example is the case of a plane steady shock hitting and reflecting from a rigid wall. Theoretically, the fluid behind the reflected shock comes to smooth flat profiles of temperature and density, and the material velocity is zero. Actually, we find that PIC leaves the fluid in a perturbed state with significant fluctuations about the constant values. These fluctuations move, roughly, with sound speed. The particles cross boundaries only infrequently if the number of them is small, so that the damping due to repartitioning is slow. Actually, the fluctuations may grow owing to the length of persistence of cell-to-cell particle number differences.

It is found that the most satisfactory results are obtained from PIC for those problems which have a general mass speed that is comparable to sound speed or greater. Systems with large positive accelerations are also well-treated.

Difficulties are generally encountered in problems with small perturbations in a fluid which is otherwise nearly at rest and in problems in which the fluid is supposed to decelerate to persistent small speeds. Further, in accelerating fluids, if material speed remains much smaller than sound speed for a time long enough for sound to travel across many cells, then poor results can be expected in the form of large fluctuations about the proper values. A number of these difficult cases are illustrated in Chapter III.

The origin of these fluctuations lies in the instability of the basic explicit Eulerian difference equations. As the fluid speed becomes small relative to the mesh, λ' of Equation (30) decreases, and the equations approach the unconditionally instable form. Small perturbations tend to grow; however, these produce local velocities which in turn increase the effective viscosity, preventing unbounded growth. If the number of particles per cell is increased, the perturbations do not grow so large, but no amount of increase of particle number can cure the difficulties. To effect a complete cure, we need a stabilizing mechanism which persists to zero speed. The requirement is for a dissipative or conductive process whose cumulative effect is proportional to cell size.

An experiment with a crude approximation to heat conduction for the most pathological cases was fairly successful, and a more refined technique of using this or similar stabilizers may make calculations of marginal problems possible. Such artificial procedures are not required for the large class of problems to which the method is suited. None of these smoothing methods was used in any of the problems reported in this paper.

3. Several Materials. Another problem concerns the pressure calculations when two or more materials are present in the system. Suppose that a cell of volume τ (one- or more-dimensional) has particles of various materials, α, which have total masses m_α. Each material occupies a fraction, σ_α (to be determined), of the volume of the cell.

$$\sum_\alpha \sigma_\alpha = 1 \tag{32}$$

For each material there is an equation of state of the form $p = f_\alpha(\rho, I)$ which can be written

$$p_\alpha = f_\alpha\left(\frac{m_\alpha}{\sigma_\alpha \tau}, I_\alpha\right) \tag{33}$$

Now, in reality, across any material discontinuity the pressure is continuous except, possibly, for certain discrete moments of time. This leads us to postulate that the pressures of all the materials in the mixed cell are always the same. Equating these, together with using Equation (32), gives just sufficient information to find the unknown quantities σ_α.

As an example, consider all the materials to be polytropic gases for which

$$p_\alpha = \frac{(\gamma_\alpha - 1) m_\alpha I_\alpha}{\sigma_\alpha \tau}$$

Equating all the p_α's to p gives

$$\sigma_\alpha = \frac{(\gamma_\alpha - 1) m_\alpha I_\alpha}{p \tau}$$

so that, from Equation (32),

$$p = \sum_{\alpha} \frac{(\gamma_{\alpha} - 1) m_{\alpha} I_{\alpha}}{\tau}$$

In this case the total pressure is just equal to the sum of the partial pressures that would be observed if the gases intermixed, each filling the whole cell. This, of course, would be true for any system of materials whose pressures are directly proportional to their densities.

Returning to the general case, we now specify that all the materials in the mixed cell have the same velocity. In reality, only the normal component of the velocity is continuous across a material discontinuity. Forcing the tangential component also to be continuous is equivalent to introducing a shear viscosity, which will be discussed in more detail in Chapter II.

In Phase I the rate of change, $\partial\Gamma/\partial t$, of the entire internal energy of the cell is calculated using an equation analogous to Equation (8). This is to be distributed among the materials such that

$$\sum_{\alpha} m_{\alpha} \frac{\partial I_{\alpha}}{\partial t} = \frac{\partial \Gamma}{\partial t} \tag{34}$$

(A separate temperature is kept for each material in a mixed cell.)

From the energy conservation equation it is seen that if pressures and velocities are the same for all materials in a close vicinity, then so is $\rho \, \partial I/\partial t$. Thus, with Λ independent of α,

$$\frac{m_{\alpha} \frac{\partial I_{\alpha}}{\partial t}}{\sigma_{\alpha} \tau} = \Lambda \tag{35}$$

Putting this into Equation (34) we obtain

$$\Lambda = \frac{1}{\tau} \frac{\partial \Gamma}{\partial t}$$

or

$$\frac{\partial I_{\alpha}}{\partial t} = \frac{\sigma_{\alpha}}{m_{\alpha}} \frac{\partial \Gamma}{\partial t} \tag{36}$$

- 21 -

Thus, each material in a mixed cell gets a different specific internal energy, allowing contact temperature discontinuities to arise.

In Phase III the incoming particles share their internal energy only with others of the same kind. In the velocity adjustment, each material shares in the internal energy increase in an amount proportional to its final mass in the cell.

Chapter II

EXTENSION OF METHOD — TWO SPACE DIMENSIONS

Several problems arise with the introduction of a new degree of freedom for the fluid motion. Some of them are demonstrated by a plane, cartesian, two-dimensional example. Others arise only with the introduction of other coordinate systems.

A. The Plane, Cartesian, Two-Dimensional Box

The box is divided into a system of square cells of side length s, in which the fluid is represented by particles. We assume for now the presence of only one kind of fluid.

Cell number $\begin{pmatrix} 0 \\ 0 \end{pmatrix}$ is the one in the lower left corner. Cell number $\begin{pmatrix} j \\ i \end{pmatrix}$ has center coordinates $\begin{pmatrix} y_j \\ x_i \end{pmatrix} = \begin{bmatrix} (j + 1/2)s \\ (i + 1/2)s \end{bmatrix}$. By this convention, which we use consistently, the cell corners have coordinates which are integer multiples of s. The velocity in cell number $\begin{pmatrix} j \\ i \end{pmatrix}$ is $\begin{pmatrix} v_i^j \\ u_i^j \end{pmatrix}$. All other previous notation is applicable here.

The density in cell $\begin{pmatrix} j \\ i \end{pmatrix}$ is
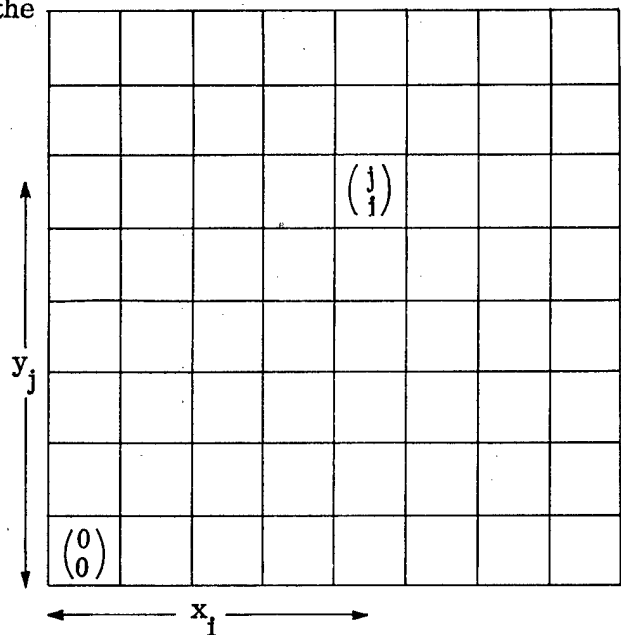
$$\rho_i^j = \frac{N_i^j m}{s^2} \tag{37}$$

so that, analogous to Equations (7) and (8), the Phase I calculations are

$$\frac{\partial u_i^j}{\partial t} = \frac{s}{2N_i^j m} \left(p_{i-1}^j - p_{i+1}^j \right) \tag{38}$$

$$\frac{\partial v_i^j}{\partial t} = \frac{s}{2N_i^j m} \left(p_i^{j-1} - p_i^{j+1} \right) \tag{39}$$

$$\frac{\partial I_i^j}{\partial t} = \frac{s}{2N_i^j m} \left[p_{i-1}^j \left(u_{i-1}^j - u_i^j \right) - p_{i+1}^j \left(u_{i+1}^j - u_i^j \right) \right.$$
$$\left. + p_i^{j-1} \left(v_i^{j-1} - v_i^j \right) - p_i^{j+1} \left(v_i^{j+1} - v_i^j \right) \right] \tag{40}$$

Values of $\tilde{u}_i^j$, $\tilde{v}_i^j$, and $\tilde{I}_i^j$ are obtained as in Equation (9).

The Phase II particle motion is again according to a velocity weighting procedure. A square of cell size is placed around each particle, and the area of overlap into each neighbor cell determines the fraction of that cell's velocity used in the movement. This is done for each component of velocity.
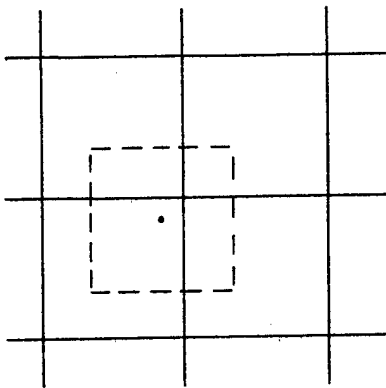
Allowance must be made for recording the passage of a particle into any of the eight neighbor cells. The repartitioning of Phase III adjusts the velocity components separately in order that no change in vector momentum occurs. Thus, for example, if one particle enters cell A from cell B, then

$$u_A^{n+1} = \frac{N_A \tilde{u}_A + \tilde{u}_B}{N_A^n + 1} \tag{41}$$

$$v_A^{n+1} = \frac{N_A^n \tilde{v}_A + \tilde{v}_B}{N_A^n + 1} \tag{42}$$

The associated change in kinetic energy is

$$\delta KE = -\frac{m}{2}\left(\frac{N_A^n}{N_A^n + 1}\right)\left[(\tilde{u}_A - \tilde{u}_B)^2 + (\tilde{v}_A - \tilde{v}_B)^2\right] \tag{43}$$

so that, analogous to Equation (13),

$$I_A^{n+1} = \frac{N_A^n \tilde{I}_A + \tilde{I}_B}{N_A^n + 1} + \frac{|\delta KE|}{m(N_A^n + 1)} \tag{44}$$

Again, if particles had also left cell A in this cycle, then the incoming particles repartition only with those that remain. Clearly, the result of repartitioning for several entering particles is independent of the order of treatment.

The one-dimensional energy considerations of Chapter I apply to this problem. The theoretical discrepancy is

$$\delta D = \frac{(\delta t)^2}{2}\sum_{ij} N_i^j m \left[\left(\frac{\partial u_i^j}{\partial t}\right)^2 + \left(\frac{\partial v_i^j}{\partial t}\right)^2\right] \tag{45}$$

Also, boundary conditions are determined by the fact that each border cell has an energy transfer to the outside of the system, which depends upon the pressure and normal velocity in the fictitious outside cell. The calculation is analogous to that leading to Equation (21).

The treatment of empty or mixed cells in this example follows as a direct extension of the procedures of Chapter I.

With regard to reflective boundaries, the two-dimensional problems introduce the following new difficulty. Suppose that a rigid obstacle with a corner is to be represented by a reflective boundary system — the edge of the shaded section. With δt small enough to satisfy the accuracy criteria, the velocity weighting assures that no particle will ordinarily enter the shaded section. The exception arises when the particle is in the section near the corner outlined by dots. There the weighting procedure can carry the particle into the shaded area no matter how small δt may be. To overcome this, a process may be used whereby the new coordinates of the particle, $\begin{pmatrix} j^{n+1} \\ j^{n+1} \\ x \end{pmatrix}$,
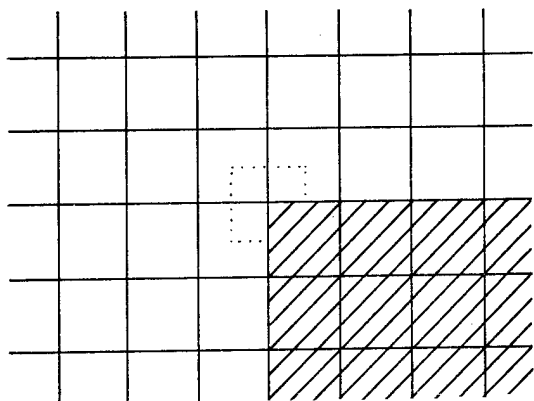
are replaced by $\begin{pmatrix} y^{n+1} \\ y_n \\ x \end{pmatrix}$ or $\begin{pmatrix} y^n \\ y_{n+1} \\ x \end{pmatrix}$, depending upon which will remove the particle from the forbidden zone.

The velocity weighting causes an effective drag area to be formed at slip lines between fluids. This is not present at boundary slip lines because of reflectivity. The drag is not dissipative nor does it propagate into the system away from the slip line as long as the slip is along a coordinate line. For diagonal slips it is not possible to construct a straight slip line, because at least some characteristics of it must stair-step along coordinate lines. What is really calculated in this case, then, is approximation to the flow past a rough boundary. This, of course, will send a signal away from the boundary whether or not viscosity is present.

By the same procedure that led to Equation (27), we may derive the lowest order statistical effect of PIC in this plane, 2-D system.

$$\rho \frac{d\vec{u}}{dt} = -\nabla p + \frac{\partial}{\partial x}\left(\lambda'_x \frac{\partial \vec{u}}{\partial x}\right) + \frac{\partial}{\partial y}\left(\lambda'_y \frac{\partial \vec{u}}{\partial y}\right) \tag{46}$$

where

$$\begin{pmatrix} \lambda'_y \\ \lambda'_x \end{pmatrix} \equiv \frac{1}{2}\rho s \begin{pmatrix} v \\ u \end{pmatrix} \tag{47}$$

The form of this result shows that the effect of repartitioning is not directly analogous to either shear or bulk viscosity in the usual sense. It does, however, have some of the properties of a real bulk viscosity but none of a real shear viscosity. There is, for example, dissipation due to compression. Several of the calculations discussed in this paper demonstrate the effects of repartitioning.

B. Problems in Other Coordinate Systems

PIC is adaptable to cylindrical, spherical, and other coordinate systems, and we have tested a variety of situations in which the configuration is independent of one of the space variables (thus 2-D problems). In these, the particles may no longer be mass points, but more complicated geometrical figures, each having a different fixed mass. A number of difficulties arise in such systems. The ways in which one can write space differences, determine boundary conditions, effect particle movement and repartitioning, etc., have been tested in only a few simple cases. The manner of making generalizations is an extensive subject requiring careful treatment; we are not presently prepared to report on any but the simplest of such situations.

The use of cylindrical coordinates for systems with azimuthal symmetry will illustrate the sort of difficulties encountered. Consider in particular the energy equation

$$\rho \frac{dE}{dt} = - \nabla \cdot (p\vec{u}) \tag{48}$$

which, in cylindrical coordinates, may be written in either of the (differentially) equivalent forms

$$\rho \frac{dE}{dt} = - \frac{1}{r} \frac{\partial(pur)}{\partial r} - \frac{\partial(pv)}{\partial z} \tag{49}$$

$$\rho \frac{dE}{dt} = - \frac{pu}{r} - \frac{\partial(pu)}{\partial r} - \frac{\partial(pv)}{\partial z} \tag{50}$$

where u and v are the velocity components in the r and z directions, respectively. When these are written in difference form, they are no longer equivalent. A criterion for choosing between them is based on the consideration of a spherical system. It can be shown that one form of difference equation from Equation (49) fails to preserve sphericity, the discrepancy being very large between corresponding cells near and far from the axis. The same form from Equation (50), however, can easily be shown to preserve sphericity. (See Chapter IV, Section C.)

Boundary conditions can be derived by considering the energy equation. With cells along the axis labeled j and those in the radial direction labeled i, the change in energy of the system in a cycle is, using difference equations from Equation (50),

$$\delta E = \delta D - \sum_{ij} \tau_i^j \, \delta t \left\{ \left[\frac{(pu)_{i+1}^j + (pu)_{i-1}^j}{2s} + \frac{(pu)_i^j}{r_i} \right] + \left[(pv)_i^{j+1} - (pv)_i^{j-1} \right] \right\} \quad (51)$$

where $\tau_i^j \equiv 2\pi r_i s^2$ (volume of cell). The axial terms cancel in pairs, leaving boundary conditions at the ends of the cylinder which are analogous to those obtained from Equation (21). Employment of a parts summation procedure for the radial terms shows that they, too, cancel in pairs; and in terms of a fictitious cell, i = −1, "within" the axis, conservation of energy requires the peculiar condition

$$(pu)_{-1}^j \equiv (pu)_0^j \quad (52)$$

together with a more complicated condition at the outside edge of the cylinder.

Arguments involving the preservation of sphericity show that the effective velocity for moving particles must be derived by area-wise weighting, as in the plane case, with no weight being given to the volume of rotation of the cell.

Chapter III

ONE-DIMENSIONAL TESTS

A number of one-dimensional tests were performed to reveal the characteristics and limitations of PIC. Most of the difficulties exposed in these tests are also present in the two-dimensional applications. The most significant results are summarized in this chapter. The calculations were performed on IBM Electronic Data Processing Machines, types 701 and 704.

A. Simple Steady-State Shock

PIC was coded for the machine calculation of a shock passing through a polytropic gas in a one-dimensional box. The left boundary of the box allowed for the inflow of gas in the shock state. The further progress of the shock was then calculated by PIC. Figures 1 and 2 show the appearance of the temperature and velocity profiles of one of the test shocks after it had traveled a number of cells. Its appearance was established quickly, and then was maintained with very little change. There were four particles per cell behind the shock and one per cell ahead. The adiabatic index was $\gamma = 5/3$. The curves were fitted by eye to pass through the value at each cell center. The shock has been smeared to a width of about two cells, one behind and one ahead. (In these and later figures, s = 1.)

As a more stringent test, the code was adapted to allow calculation for two gases, both initially cold and at rest. They were of different densities. The same shock as above was fed in from the left and allowed to develop its steady-state configuration before hitting the other gas. The results at late times are shown in Figures 3 and 4 for the case in which the second gas was much lighter (rarefaction reflected) and in Figures 5 and 6 for the case in which the second gas was much heavier (shock reflected).

In these shock problems, the smoothness of the velocity profiles is an indication of the proper entropy production across the shock. The smearing

of the shock width is no greater than that produced by other finite difference methods. The method of treating contact discontinuities varied in slight detail from that which is described in Chapter I.

B. The Closed One-Dimensional Box

A machine code was devised which would calculate the configuration changes of one or two fluids in a closed one-dimensional box. One of these fluids, A, was a polytropic gas; the other, B, could have any equation of state within rather wide limitations.

1. The Shock Tube. This problem constitutes a stringent test for one-dimensional calculation procedures, since a shock, a rarefaction, and a contact discontinuity must all be represented.

Only the gas was put in the tube; initially it was at rest and uniform temperature. A diaphragm separated two regions which were at different density and pressure (we take the high density to be on the left). At $t = 0$, the diaphragm ceases to exist, and a rarefaction then moves leftward while the contact discontinuity and a shock travel to the right. Before the disturbances hit the walls of the box, there is no characteristic length in the system, so that the effect of changing cell size is only to change the time scale. The only artificial parameter that can be varied for a given initial physical situation is N, the average number of particles per cell. Several interesting features are observed from the resulting velocity profile:

(a) The initial perturbations in the system, resulting from the way in which the problem was started, introduced an oscillatory pattern superimposed on the correct velocity profile. This means insufficient entropy production in the early stages. The fluctuations travel with the shock front, not increasing in amplitude. At any fixed position, they die out, and the velocity comes to its proper value. These results are shown in Figure 7 for the initial configuration of a 5-to-1 density ratio, $\gamma = 5/3$.

(b) Increasing the number of particles per cell everywhere (maintaining the same initial density ratio) reduces the amplitude of the fluctuations. In (a), there were intially five particles per cell on the left and one per cell on the right. Multiplying these numbers by two produces roughly one-half the amplitude of oscillations at any stage of the calculation but otherwise leaves the rarefaction appearance, plateau height, and shock speed the same.

(c) Smaller initial density ratios across the diaphragm produce relatively greater oscillations. A problem with 2-to-1 ratio (two particles per cell on the left, one per cell on the right) produced tremendous oscillations,

200 to 300 per cent of the true velocity. Multiplying the number of particles by six reduced the fluctuations to an amplitude of less than 50 per cent of the true velocity. In both cases, however, the oscillations were centered about the true plateau, and the rarefaction and shock speeds were well produced. This fact is significant in that it demonstrates that PIC is stable to very large fluctuations and that these fluctuations, even when extreme, tend in the average to produce the gross configuration features.

     2. Gravity Problems. Again, only the gas was in the tube, this time at constant density and temperature and at rest everywhere. The box was 100 cells long and closed (reflective) at each end. An acceleration field of magnitude g was applied to the right. Until an element of material feels the signal from the wall, it accelerates uniformly, and the velocity profile remains perfectly flat. Theoretically, a shock is formed at a distance $c^2/2g$ back of the wall (c is the material sound speed). At the left end, a rarefaction is produced. As discussed in Chapter I, the material which comes to rest at the right end will not be treated well; we do, indeed, observe residual fluctuations. The smoothness of the rarefaction zone, however, depends upon the magnitude of the acceleration. If this is small, the slow-speed fluctuations have a chance to become appreciable; if it is large, then no fluctuations appear. Smoothness seems to require $c^2/sg \lesssim 10$. This, unfortunately, means that at the end where material piles up, a shock theoretically will be formed at a distance back of the end somewhat less than 1/10 s. These results put severe restrictions on doing gravity problems with PIC. No cure for these difficulties is effected by decreasing δt, the time for a cycle.

   Two typical examples are shown in Figure 8. Even in the fluctuating example, the curve is tolerably smooth at the higher velocities (>half of sound speed), showing that perturbations to the flow do not grow in rapidly moving systems. The smoother curve was allowed to develop four times longer than at the time shown. By then, a large cavity had formed at the left, and the rarefaction wave was still smooth. The shocked region was by then quite thick and poorly represented. Profiles at typical later times are shown in Figure 9.

     Experiments also showed that a small perturbation introduced into the middle of the box grows if c^2/sg is much larger than around 10, and otherwise it damps. Increasing the number of particles per cell does not cure the situation, either here or in the rarefaction.

     The case of infinite acceleration was accomplished by running the problem of a gas escaping into a vacuum; the results showed good agreement with the theoretical rarefaction profile.

3. Coarse Zoning Test. A clear demonstration of the qualitative discrepancies that can occur when zoning is coarse is given by the following example:

The box is in three sections; from left to right are fluid A, fluid B, and vacuum. Initially, the two fluids have the same pressure and both are moving to the right with the same speed. One expects fluid B to rarify at first, then compress, and heat as it crowds against the right end. A shock should then propagate back through fluid A. These qualitative features are observed if the zoning is such that fluid B, when most compressed against the end, occupies more than one cell. If, however, fluid B is all compressed into one cell, then a vast qualitative difference is observed from that expected. The cell of fluid A next to the hot, crowded, fluid-B cell drops in temperature when it should rise; its temperature becomes negative. No shock pulse is sent back into fluid A until the negative temperature is sufficiently raised by repartitioning of the returning fluid B, but this is much too late. These features are as predicted in Chapter I.
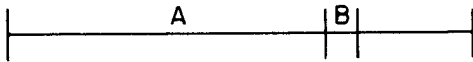
C. Expanding Spheres

Two companion spherically-symmetric calculations (one-dimensional in spherical coordinates) were run under the following code names:

OBOE, using the spherical form of PIC.
ROBOE, using well known Lagrangian hydrodynamic methods.

The problems started with the following configurations. Three concentric spheres of radii 5, 20, and 30 marked the boundaries separating, respectively, a central piston (not zoned), perfect gas A, perfect gas B, and a vacuum. The gases were initially cold and at rest. Gas A was much less dense than gas B.

The situation was generated by allowing the piston to expand, at first accelerating, then with nearly constant velocity, then decelerating.

ROBOE was run first; some of the observed features are shown in Figures 10 and 11. In order that the OBOE problem have the same input at the piston the following procedure was adopted: The "piston cell" was defined as the cell with the piston, except that if that cell has no particles, then the piston cell included also the next cell beyond. The input data included both the piston speed and the total energy of ROBOE as functions of time. The particles in the piston cell were forced to have the piston speed.

Knowing the kinetic energy input that this produced per cycle, we subtracted this from the total energy that should have been added according to ROBOE and inserted the difference as internal energy increase to the particles in the piston cell. This was equivalent to having a heat conduction at the OBOE piston to insure the same boundary conditions there as in ROBOE. This did not in itself force agreement between OBOE and ROBOE in any other respects.

The energies of OBOE are shown in Figures 10 and 11, together with those of ROBOE. Note the large relative fluctuation of internal energy in OBOE at early times. The momentary negative internal energy arose because the true thickness of material which should have the piston speed was somewhat less than the width of the piston cell.

There is some difference between the times at which the kinetic energy in gas B began to rise. This can be traced directly to the fact that the shock front was steeper in OBOE than in ROBOE. The initial rise in B kinetic energy in ROBOE was due to the precursor ahead of the shock. This is well shown by Figure 12 where the velocity profiles for the two problems are shown at a time just before the shock hit B, and by Figure 13 which presents the motion of the A-B boundary for the two problems as a function of time. It is not known which calculation more closely reproduced the true physical picture.

The two temperature profiles are shown in Figure 14 for a time which is the same as in Figure 12. Figures 15 and 16 show velocity and temperature profiles, respectively, for a rather late time in the problems.

Chapter IV

TWO-DIMENSIONAL CALCULATIONS

Various two-dimensional calculations have been performed with PIC; several of those which demonstrate the characteristics and capabilities of the method are discussed here. An unfortunate feature of these problems is that no solutions for comparison are available except in the simplest cases.

A. The SUNBEAM Code

Two different polytropic gases are arranged in arbitrary configuration in a plane, two-dimensional, rectangular box, the sides of which are rigid (reflective) boundaries. SUNBEAM then calculates the changes of configuration in the manner discussed in Chapter II. A number of different kinds of calculations can be done with such a code. Two examples follow.

1. Interface Motion Studies. Figure 17 shows the rectangular box, together with the interface between gases at various times. Initially, the gas at the right was of low density, but very hot so as to have a high pressure compared with the fluid to the left which was of greater density but cold. There were four particles in each cell at the start.

A number of variations have been run. No apparent difficulties have arisen in the calculations; the results agree with the qualitative predictions that one can make.

2. Cylindrical Shock Pulse. Figures 18 to 21 show a sequence of particle configurations resulting from the following initial conditions: The two gases (simulating air and ground except that the density ratio was 1 to 20) were both at the same pressure, at constant densities, and cool except that within a circular segment of five cells radius in the upper right corner, the temperature was 100 times greater than in the rest of the air. (Those cells that were cut by the circle had appropriate fractions of the large

central temperature.) Again, there were no computational difficulties in running this problem.

B. The KAREN Code

A single polytropic gas is confined in a plane, two-dimensional, rectangular box, the top and bottom of which are rigid (reflective). Horizontally, the system is considered to be one period of an infinite periodic system. This is accomplished by taking for the conditions in the fictitious cells just to the right or left of the box, the conditions just on the inside of the corresponding other side. Also, particles passing out across one boundary, pass in across the other. Further, a fixed, rigid (reflective) object of arbitrary shape (as long as its boundaries follow cell boundaries) can be placed anywhere in the box. Initially, the gas may be homogeneous in temperature, density, and velocity (moving, say, to the right at a specified initial Mach number), or the gas may commence motion from rest under a horizontal acceleration field. A large number of problems have been run for various initial situations. An example will typify the kinds of results: The box was square, 20 cells on a side. The obstacle, attached to the bottom, was a rectangle 10 cells high by 6 cells wide. Initially, the gas was homogeneous, moving to the right at near Mach 2. Figures 22 and 23 show, respectively, the horizontal and vertical momenta of the gas as functions of time.

Problems have been run in which the obstacle was placed symmetrically in the center of the box. The flow remained symmetric until a slight perturbation was introduced, whereafter vertical oscillations in momentum grew to much greater than the perturbation intensity and showed a frequency from which a very reasonable Strouhal number could be derived.

C. Cylindrical Coordinates

In connection with the cylindrical-coordinate procedure discussed in Chapter II, we mention one problem that was designed to test the preservation of sphericity. This was the calculation of an expanding sphere of hot gas moving under its internal pressure into a cold gas of uniform initial density. After the central gas had expanded to more than three times its original radius, the deviations from sphericity were around 3 per cent. Figure 24 shows the initial boundary between the gases, together with the final particle configuration. The larger dotted line is a circular segment; the heavy line separates particles of the two materials.

With this coarseness of mesh and small number of particles, deviations are expected to be relatively large. Similar calculations with much finer zoning and many more particles do give better results.

Appendix I

OTHER METHODS FOR SOLVING 2-D PROBLEMS

There is a large difference in difficulty between 1-D and 2-D hydro-dynamic problems, but any successful procedure for solving 2-D problems is likely to give relatively little difficulty when it is being applied to the analogous 3-D problems. Here we discuss briefly some other methods for solving 2-D problems:

1. <u>Moveable Coordinate (Lagrangian) Methods</u>. The essential feature of these methods is that the coordinate system is a mesh of cells imbedded in the fluid and moving with it. A typical application has each corner of the mesh carrying a certain fixed mass of fluid as well as pressure, position, and velocity which vary with time. The appropriate differential equations are written in a finite difference approximation form and advancements of the configuration in time are thereby related to space differences.

The Lagrangian approach has proved particularly useful for treating systems involving several fluids, because each mesh point always retains identity with its initial portion of the fluid. The interfluid boundaries are always clearly delineated. A large number of strikingly successful calcula-tions have been performed by several groups of workers.

The Lagrangian methods are limited, however, to use with systems in which no large distortions of the fluid occur. In a finite-size mesh, various topological catastrophes can happen which reduce further results to nonsense. Indeed, rather serious doubt is cast upon the accuracy of representing the true solution when, for example, a system whose equations were based on an orthogonal mesh becomes distorted significantly away from orthogonality.

Problems involving oblique collision of two free surfaces are difficult to solve by Lagrangian methods.

2. Fixed Coordinate (Eulerian) Methods. The essential feature of fixed coordinate methods is that the coordinate system is not tied to the fluid; usually it is stationary in the laboratory frame of reference. Strict application of this approach allows no identification of the fluid elements. Each cell of the mesh is characterized by uniform density, pressure, "color" (i.e., designation of material kind), and velocity. Thus, finite space differencing procedures for representing the differential equations can retain equal applicability throughout a wide range of fluid distortions.

The principal difficulty with the strict Eulerian methods is that they tend to introduce false diffusions, especially noticeable with material boundaries. This arises from the fact that each cell is forced to be homogeneous; when material enters a cell, its characteristics are uniformly mixed with those of all the other materials in the cell.

3. Mixed Euler-Lagrange Systems. Many modifications have been proposed—some have been tried—which take advantage of the better features of both fixed and moveable coordinates. These include: (a) Fixed coordinates in one direction, moveable in the other. Usually, advantage is taken of the prior knowledge of slip-line positions. (b) Fixed coordinates but with, in addition, a special Lagrangian treatment of interfluid boundaries. (c) Two superimposed coordinate systems—an Eulerian one for calculating and advancing field functions and a Lagrangian one for keeping track of the positions of material points. This procedure is generally somewhat extravagant in the use of memory space in the computing machine.

4. Repulsive-Particle Methods. The fluid is represented by a system of mass points of fixed mass whose coordinates vary with time. The pressure in the fluid is represented by prescribing some repulsive interparticle force which is a function of separation.

For example, the pressure in a polytropic gas in n-dimensional space can be represented by an interparticle repulsive force

$$F_{ij} = \frac{-\partial}{\partial r_{ij}} \left[\frac{const.}{(r_{ij})^{n(\gamma - 1)}} \right]$$

where γ is the adiabatic exponent of the gas, and the constant varies with entropy.

Many problems arise in the practical application of these and any other methods for solving the differential equations of motion. Some of the difficulties are the following.

1. Stability of the difference equations. Instabilities may arise from several sources which include: (a) Having too large finite time interval per cycle—the classical "Courant instability." (b) Failure of the method when an attempt is made to treat a situation of a type which the method is not capable of handling. (c) Boundary instabilities. Free surfaces in Lagrangian methods may be troubled by instability. The method presented in this report can suffer from a peculiar boundary instability under certain conditions.

2. The production of entropy. In order to allow for the presence of shocks without special treatment, a dissipative mechanism must be present in the difference equations. This is usually achieved in two ways: (a) An artificial viscosity may be introduced into the equations. (b) The truncation errors of the finite difference approximation can, under certain circumstances, automatically provide sufficient dissipation.

Some success has been achieved by actually keeping track of shock boundaries separately and relating field functions on both sides by the proper conservation conditions.

3. Accuracy of representation of the solution of the differential equations. There is no guarantee that making the finite difference intervals smaller and smaller will produce convergence to the true solution. Many authors have devoted a large amount of analysis to this and related topics. Every slight variation of procedure within the framework of any one method must be examined for its contribution to inaccuracies.

Appendix II

AN ALTERNATIVE DERIVATION OF THE PIC DIFFERENCE EQUATIONS

by Eleazer Bromberg

Introduction

This section presents a derivation of PIC which emphasizes the role of Lagrangian and Eulerian concepts. This approach may help to develop variant numerical techniques when needed.

We shall assume for simplicity that the boundary of the domain D under study is fixed and that no fluid crosses it; the resulting equations can easily be modified to take account of different boundary conditions. We shall also assume that we are dealing with a single material, characterized by a single equation of state relating the values of density ρ, pressure p, and specific internal energy I of the material.

As in the customary Lagrangian formulation, the time rate of change of position of a point in the fluid is equal to the velocity

$$\dot{x} = \frac{dx}{dt} = u(x, t) \tag{A-1}$$

where x and u may be considered as scalars in one-dimensional problems or as vectors $\{x_i\}$ and $\{u_i\}$ in two or more dimensions. Integration of Equation (A-1) yields

$$x = x(x_0, t) \tag{A-2}$$

the position of any given point in the fluid as a function of time t and its initial position x_0.

A. Mass and Density

The density distribution at time t, $\rho(x, t)$, must satisfy the mass-conservation law which we write in integral form

$$\int_V \rho(x, t)dV = \int_{V_0} \rho_0(x_0)dV_0 \qquad \text{(A-3)}$$

where V is any region fixed in the fluid, V_0 is its initial volume, ρ_0 is the initial density distribution, and dV and dV_0 are corresponding elements of volume. This yields the alternate form of the mass-conservation law

$$\rho = \rho_0 \frac{dV_0}{dV} = \rho_0 \, J\left(\frac{x_0}{x}\right) \qquad \text{(A-4)}$$

where dV_0/dV is the Jacobian in multidimensional cases.

We now introduce the assumption that ρ_0 is to be represented by a delta function; that is, by a function which differs from zero only at a finite number of points x_{0k}, and which rises to infinity at each of those points in a manner such that the volume integral of the density in any sufficiently small neighborhood enclosing a particular point is a constant characteristic of the point but independent of the size or shape of the volume element. This constant is referred to as the "mass of the particle" associated with the point in question. These masses are chosen so as to satisfy the conservation law:

$$M = \int_D \rho(x, t)dV = \int_D \rho_0(x_0)dV_0$$

$$= \sum_{k=1}^{n} \int_{D_k} \rho_0(x_0)dV_0$$

$$= \sum_{k=1}^{n} m_k \qquad \text{(A-5)}$$

where D is the entire domain, which is considered to be divided up into n subdomains D_k such that each subdomain encloses only one point at which ρ_0 is other than zero. For any arbitrary volume V, we obtain

$$\int_V \rho(x, t)dV = \int_{V_0} \rho_0(x_0)dV_0 = \sum m_j \qquad \text{(A-6)}$$

where the sum is taken over those particles to be found in the volume V at time t. This volume may be so chosen as to be empty of particles at time t, in which case the value of the corresponding integral will be zero. However, this does not interfere with the validity of the conservation law in the large.

B. Solving the Dynamical Equations

Having established the characteristics of the density function, we can turn to the momentum and energy conservation laws and develop the computational process based on the above considerations.

We assume that the domain D is covered by a mesh which is chosen so as to lead to simple expressions for the difference quotients representing such quantities as gradient, divergence, and normal derivative associated with any cell of the mesh. The mesh distribution does not, in general, have any special relation to the subdomains in the previous section. The density associated with any cell c is obtained from Equation (A-6) by approximating the integral on the left:

$$\int_{V_c} \rho\, dV = \rho_c\, V_c \qquad \text{(A-6')}$$

from which it follows that

$$\rho_c = \frac{1}{V_c} \sum_{V_c} m_j \qquad \text{(A-6'')}$$

In the process of integration, we treat the mesh as Lagrangian at the beginning of each time cycle, allowing each cell to be displaced, but then

we immediately rezone so as to return to the original spatial mesh distribution. Thus, each time cycle of integration of the momentum and energy conservation equations is divided into two parts. In one, we deal with each cell of the mesh as fixed in the fluid rather than in space to determine its change of momentum and energy; this displaces its boundaries. In the second phase, we rezone the cells (and mass points) in order to reintroduce the original mesh distribution; in the process, we repartition momentum and energy so as to obtain new spatial distribution functions without affecting the conservation of these quantities. The initial mesh structure is, therefore, kept fixed in the sense that it reappears at the end of each integration cycle. This method is, consequently, not subject to the difficulties which normally arise in the Lagrangian method as a consequence of the distortion of the Lagrangian cells. We shall henceforth label the cells considered to be fixed in the fluid L_i, and those fixed in space E_i.

Phase I

The momentum and energy conservation laws can be written as follows:

$$\frac{d}{dt} \int_D \rho u \, dV = - \int_{S_D} pn \, dS \tag{A-7m}$$

$$\frac{d}{dt} \int_D \rho e \, dV = \frac{d}{dt} \int_D \rho(I + \frac{1}{2}u^2) dV = - \int_{S_D} (pu)_n \, dS \tag{A-7e}$$

where

e = the specific total energy
I = the specific internal energy
dS = a surface element
$(pu)_n$ = the normal component of pu
$n(x,t)$ = the unit outward normal to the surface
S_D = the surface bounding volume D.

A similar set of equations applies to each cell of the mesh:

$$\frac{d}{dt} \int_{L_i} \rho u \, dV = - \int_{SL_i} pn \, dS \tag{A-8m}$$

- 42 -

$$\frac{d}{dt} \int_{L_i} \rho I \, dV + \frac{d}{dt} \int_{L_i} \frac{1}{2} \rho u^2 \, dV = - \int_{SL_i} (pu)_n \, dS \qquad \text{(A-8e)}$$

but the volumes L_i and their surfaces SL_i are now functions of time, though they coincide with the fixed mesh at time t.

Integrating Equations A-8 between times t and t + δt, we obtain

$$\int_{L_i(t+\delta t)} \rho u \, dV = \int_{L_i(t)} \rho u \, dV - \int_t^{t+\delta t} \int_{SL_i(t)} pn \, dS \, dt \qquad \text{(A-9m)}$$

$$\int_{L_i(t+\delta t)} I \, dV = -\frac{1}{2} \left[\int_{L_i(t+\delta t)} \rho u^2 \, dV - \int_{L_i(t)} \rho u^2 \, dV \right] + \int_{L_i(t)} \rho I \, dV$$

$$- \int_t^{t+\delta t} \int_{SL_i(t)} (pu)_n \, dS \, dt \qquad \text{(A-9e)}$$

in which each integrand is to be evaluated over the indicated domain at the indicated time. There is considerable latitude in choosing the particular formula for evaluating the integrals in (A-9) numerically. In the present report, we use the following prescriptions:

(a) The integrals over time are set equal to the value of the integrand at the time corresponding to the lower limit of t, multiplied by δt; that is,

$$\int_t^{t+\delta t} \int_{SL_i(t)} pn \, dS \, dt = \delta t \int_{SL_i(t)} pn \, dS \qquad \text{(A-10m)}$$

$$\int_t^{t+\delta t} \int_{SL_i(t)} (pu)_n \, dS \, dt = \delta t \int_{SL_i(t)} (pu)_n \, dS \qquad \text{(A-10e)}$$

(b) The volume integrals, which are all of the form $\int_{L_i(\tau)} \rho f \, dx$,

where f is any function of x and τ may be either t or t + δt, shall be evaluated as:

$$\int_{L_i(\tau)} \rho f \; dV = f_{L_i}(\tau) \int_{L_i(\tau)} \rho \; dV \qquad\qquad \text{(A-11)}$$

where $f_{Li}(\tau)$ is the value of f associated with the cell L_i at time τ. Since the L_i are being treated as Lagrangian cells,

$$\int_{L_i(t)} \rho \; dV = \int_{L_i(t+\delta t)} \rho \; dV = \sum_{L_i} m_j = M^n_{L_i}$$

the summation being taken over the mass points located within the cell L_i.

The superscript n identifies the cycle of time integration (and hence the time t). We use the following nomenclature for f:

$$f_{L_i}(t) = f^n_{L_i}$$

$$\text{(A-12)}$$

$$f_{L_i}(t + \delta t) = \tilde{f}_{L_i}$$

The numerical integration formulae for Equations (A-8) [or (A-9)] can, therefore, be written as

$$M^n \tilde{u} = M^n u^n - \delta t \int_S pn \; dS \qquad\qquad \text{(A-13m)}$$

$$M^n \tilde{I} = -\frac{1}{2} M^n \left[(\tilde{u})^2 - (u^n)^2 \right] + M^n I^n - \delta t \int_S (pu_n) \; dS$$

$$\text{(A-13e)}$$

The subscript L_i is understood to be associated with each quantity in (A-13).

In general, the values of the integrand in the surface integrals must be chosen so that when the Equations (A-13) are summed over all the cells L_i of the domain D, the sum of these integrals shall yield just the surface integral over the bounding surface SD. This implies that the contributions of the surface integrals shall cancel at interfaces of adjacent cells (even if one or more of these cells are empty of mass points). In the present programs, the values of the integrand are determined from the relations

$$[p]_{\text{at surface}} = p_{L_i} + \frac{s}{2} \frac{\partial p}{\partial n}$$

$$[pu_n]_{\text{at surface}} = p_{L_i} (u_{L_i})_n + \frac{s}{2} \frac{\partial}{\partial n} (pu_n) \qquad \text{(A-13')}$$

Each normal derivative is represented by a centered difference quotient, that is, by the difference in the values of the quantity in properly chosen opposite neighbors divided by the distance between the centers of these cells. Account must be taken of the fact that $(u_{L_i})_n$ will have the same absolute value, but opposite sign, for any two opposed bounding surfaces of a cell.

Phase II

1. Rezoning of Cells. Having determined the change of velocity and specific internal energy associated with the Lagrangian cell L_i during the interval δt, we wish to rezone; that is, to determine corresponding quantities associated with cells (which we shall call E_i) occupying the same spatial positions as $L_i(t)$ [or $L_i(o)$, for that matter].

For this purpose, we note that for any function $g(x,t)$ defined over a cell L_i, at any time t,

$$\frac{d}{dt} \int_{L_i(t)} \rho g \, dV = \frac{d}{dt} \int_{E_i} \rho g \, dV + \int_{SE_i} \rho g \, u_n \, dS \qquad \text{(A-14)}$$

where E_i is taken to be a fixed volume, equal to $L_i(t)$, and SE_i is the surface of E_i.

Integrating Equation (A-14) with respect to time, we obtain

$$\int_{L_i(t+\delta t)} \rho g \ dV - \int_{L_i(t)} \rho g \ dV = \int_{E_i} \rho(x, t+\delta t) \ g(x, t+\delta t) \ dV$$

$$- \int_{E_i} \rho(x, t) \ g(x, t) \ dV$$

$$+ \int_t^{t+\delta t} \int_{SE_i} \rho g \ u_n \ dS \ dt \qquad \text{(A-15)}$$

Since $E_i = L_i(t)$,

$$\int_{L_i(t)} \rho g \ dV = \int_{E_i} \rho(x, t) \ g(x, t) \ dV \qquad \text{(A-16)}$$

and the corresponding terms in Equation (A-15) cancel.

We now apply Equation (A-11) to the integral over E_i, and we use the labels

$$g_{E_i}(t+\delta t) = g_{E_i}^{n+1}$$

$$\text{(A-17)}$$

$$\int_{E_i} \rho(x, t+\delta t) \ dV = \sum_{E_i} m_j = M_{E_i}^{n+1}$$

The expression (A-15) can be written as

$$M_{E_i}^{n+1} g_{E_i}^{n+1} = M_{L_i}^n \widetilde{g}_{L_i} - \int_t^{t+\delta t} \int_{SE_i} \rho g \ u_n \ dS \ dt \qquad \text{(A-18)}$$

or, since $M_{L_i}^n = M_{E_i}^n$,

$$M_{E_i}^{n+1} g_{E_i}^{n+1} = M_{E_i}^n \widetilde{g}_{L_i} - \int_t^{t+\delta t} \int_{SE_i} \rho g \, u_n \, dS \, dt \qquad \text{(A-19)}$$

The surface integral corresponds to the transport of g from one cell to the other, resulting from the motion of the fluid. As in Phase I, it must be evaluated in a manner such that the contributions of adjacent cells over their common interface are equal and opposite. This can be done in various ways; in the current computations, we replace g by $\widetilde{g}_{L_i}$ so that the surface integral becomes:

$$\int_t^{t+\delta t} \int_{SE_i} \rho g \, u_n \, dS \, dt = \widetilde{g}_{L_i} \int_t^{t+\delta t} \int_{SE_i^*} \rho u_n \, dS \, dt$$

$$- \sum_N \widetilde{g}_{L_i N} \int_t^{t+\delta t} \int_{SE_i^{**}} \rho |u_n| \, dS \, dt \qquad \text{(A-20)}$$

where the first integral on the right hand side is taken over those parts of the surface where u_n is positive (the flow is out), and the second is taken over those parts where the flow is inward. The quantity $g_{L_i N}$ is that of the neighboring cell from which the flow is entering. The integrals yield the mass of material entering or leaving E_i in accordance with the recipe prescribed in Equation (A-6). This can be seen more readily by replacing u_n dt by dx_n; the latter is the component of the displacement of the fluid in time dt normal to the surface element dS. The product dx_n dS is the volume of fluid passing through dS in time dt. A typical integral can, therefore, be written as

$$\int_t^{t+\delta t} \int_{SE_i} \rho u_n \, dS \, dt = \int_t^{t+\delta t} \int_{SE_i} \rho \, \delta V \qquad \text{(A-21)}$$

- 47 -

where δV is used to indicate the special character of this element of volume. Transforming in accordance with Equation (A-6), we get

$$\int_t^{t+\delta t} \int_{SE_i} \rho\, \delta V = \int_t^{t+\delta t} \int_{SE_i} \rho_0\, \delta V_0 = \sum_{SE_{i,\delta t}} m_j \qquad (A-22)$$

that is, the sum of the masses of the particles whose location has crossed SE_i in time δt.

Summarizing Equations (A-19), (A-20), and (A-21), we obtain the typical rezoning (or repartitioning) equation

$$M_{E_i}^{n+1} g_{E_i}^{n+1} = M_{E_i}^n \tilde{g}_{L_i} - \tilde{g}_{L_i} \sum_{out} m_j + \sum_N \tilde{g}_{L_iN} \sum_{in} m_{j,N}$$

$$= \left(M_{E_i}^n - \sum_{out} m_j \right) \tilde{g}_{L_i} + \sum_N \left(\tilde{g}_{L_iN} \sum_{in} m_{j,N} \right) \qquad (A-23)$$

where the last summation is over those neighboring cells from which particles have entered E_i. In the particular cases of momentum and energy, the corresponding expressions are

$$M^{n+1} u^{n+1} = \left(M^n - \sum_{out} m_j \right) \tilde{u} + \sum_N \left(\tilde{u}_N \sum_{in} m_{j,N} \right) \qquad (A-24m)$$

$$M^{n+1} e^{n+1} = \left(M^n - \sum_{out} m_j \right) \tilde{e} + \sum_N \left(\tilde{e}_N \sum_{in} m_{j,N} \right) \qquad (A-24e)$$

The appropriate cell subscripts can be determined from Equation (A-23). The second of these (A-24e) is generally written so as to solve for I^{n+1}; namely,

$$M^{n+1} I^{n+1} = \left(M^n - \sum_{\text{out}} m_j \right) \widetilde{I} + \sum_N \left(\widetilde{I}_N \sum_{\text{in}} m_{j,N} \right)$$

$$+ \frac{1}{2} \left[\left(M^n - \sum_{\text{out}} m_j \right) \widetilde{u}^2 + \sum_N \left(\widetilde{u}_N^2 \sum m_{j,N} \right) - M^{n+1} \left(u^{n+1} \right)^2 \right] \qquad \text{(A-24e')}$$

    2. <u>Relocation of Mass Points.</u> In order to determine those mass points which cross any cell interface in time δt, it is necessary to keep track of the positions of the mass points. This is accomplished by integrating Equation (A-1) during each time cycle:

$$\delta x_k = u_k \, \delta t \qquad \text{(A-25)}$$

or

$$x_k^{n+1} = x_k^n + u_k \, \delta t \qquad \text{(A-25')}$$

where the subscript k is used to identify each mass point and x_{ok} as its initial position, as described at the beginning of this Appendix.

    It is important to note that the Lagrangian formulation of the equations of fluid flow (which are being used here) has as one of its basic assumptions that any small volume element fixed in the fluid remains a small volume element throughout the motion and always includes the same points of the fluid, although its shape and size may be altered to some extent. This is equivalent to the requirement that the mass points do not pass each other as originally prescribed in the description of PIC. This condition is satisfied if δt is sufficiently small and if $u(x, t)$ is represented by a continuous function when used to determine the position of the mass points as in Equation (A-25) or (A-25'). The value of u_k used in Equation (A-25') may be obtained by some form of interpolation among the values of the cell velocity for groups of neighboring cells using either $u_{E_i}^n$, $\widetilde{u}_{L_i}$, $u_{E_i}^{n+1}$, or some combination of these quantities. An effective method of interpolation is presented in the body of this report (Chapter II). It can be described generally by the formula

$$(u_k)_{eff} = \alpha_{k_o} \tilde{u}_{L_i} + \sum_{j=1}^{3} \alpha_{k_j} \tilde{u}_{L_i j} \qquad \text{(A-26)}$$

where $\sum_{j=0}^{3} \alpha_{k_j} = 1$, the α_{k_j} are weight functions, and $L_i j$ refers to the three neighboring cells.

C. Summary

The computational procedure can be summarized as follows:

We start with a suitably chosen mesh, a set of mass points, and the values of the mass, velocity, and specific internal energy associated with each cell. (The mass associated with each cell must be equal to the sum of the masses of the mass points located in that cell.) Given these data at the end of the n-th time cycle (which may be the initial time), we obtain the corresponding values at the end of the (n + 1)st time cycle by solving the following systems of equations:

1. For each cell:

$$p = p(I, \rho) \qquad \text{(A-27)}$$

the equation of state, where

$$\rho = \sum_c \frac{m_j}{V_c} = \frac{M_c^n}{V_c} \qquad \text{(A-6'')}$$

where V_c is the volume of the cell, and

$$\tilde{u} = u^n - \frac{\delta t}{M^n} \int_{S_e} pn \, dS \qquad \text{(A-13m)}$$

$$\widetilde{I} = -\frac{1}{2}\left[(\widetilde{u})^2 - (u^n)^2\right] + I^n - \frac{\delta t}{M^n}\int_{S_c}(pu)_n\, dS \qquad \text{(A-13e)}$$

in which the surface integrals may be evaluated by any one of several methods described elsewhere. These methods must always be consistent with over-all conservation laws and generally also have to provide for such contingencies as "empty" cells and special types of boundaries (such as the axis of symmetry in cylindrical problems).

2. For each mass point:

$$x^{n+1} = x^n\, u_{eff}\, \delta t \qquad \text{(A-25'')}$$

where u_{eff} has the form

$$u_{eff} = \alpha_{k_o}\, u_{L_i o} + \sum_{j=1}^{N}\alpha_{k_j}\, u_{L_i j} \qquad \text{(A-28)}$$

$$\sum_{j=0}^{N}\alpha_{k_j} = 1 \qquad \text{(A-29)}$$

and $u_{L_i o}$ is a velocity associated with the cell in which the point is located, $u_{L_i 1}$ to $u_{L_i N}$ are similar velocities associated with neighboring cells, and the α_{k_j} are weight functions.

For each cell:

$$M^{n+1} = M^n - \sum_{out} m_j + \sum_{in} m_{j,N} \qquad \text{(A-30)}$$

$$u^{n+1} = \frac{1}{M^{n+1}}\left[\left(M^n - \sum_{out} m_j\right)\widetilde{u} + \sum_{N}\left(\widetilde{u}_N \sum_{in} m_{j,N}\right)\right] \qquad \text{(A-24m')}$$

$$I^{n+1} = \frac{1}{M^{n+1}} \left[\left(M^n - \sum_{out} m_j \right) \widetilde{I} + \sum_N \left(\widetilde{I}_N \sum m_{j,n} \right) \right.$$

$$\left. + \frac{1}{2} \left\{ \left(M^n - \sum_{out} m_j \right) \widetilde{u}^2 + \sum_N \left(\widetilde{u}_N^2 \sum_{in} m_{j,N} \right) \right\} \right] \qquad \text{(A-24e'')}$$
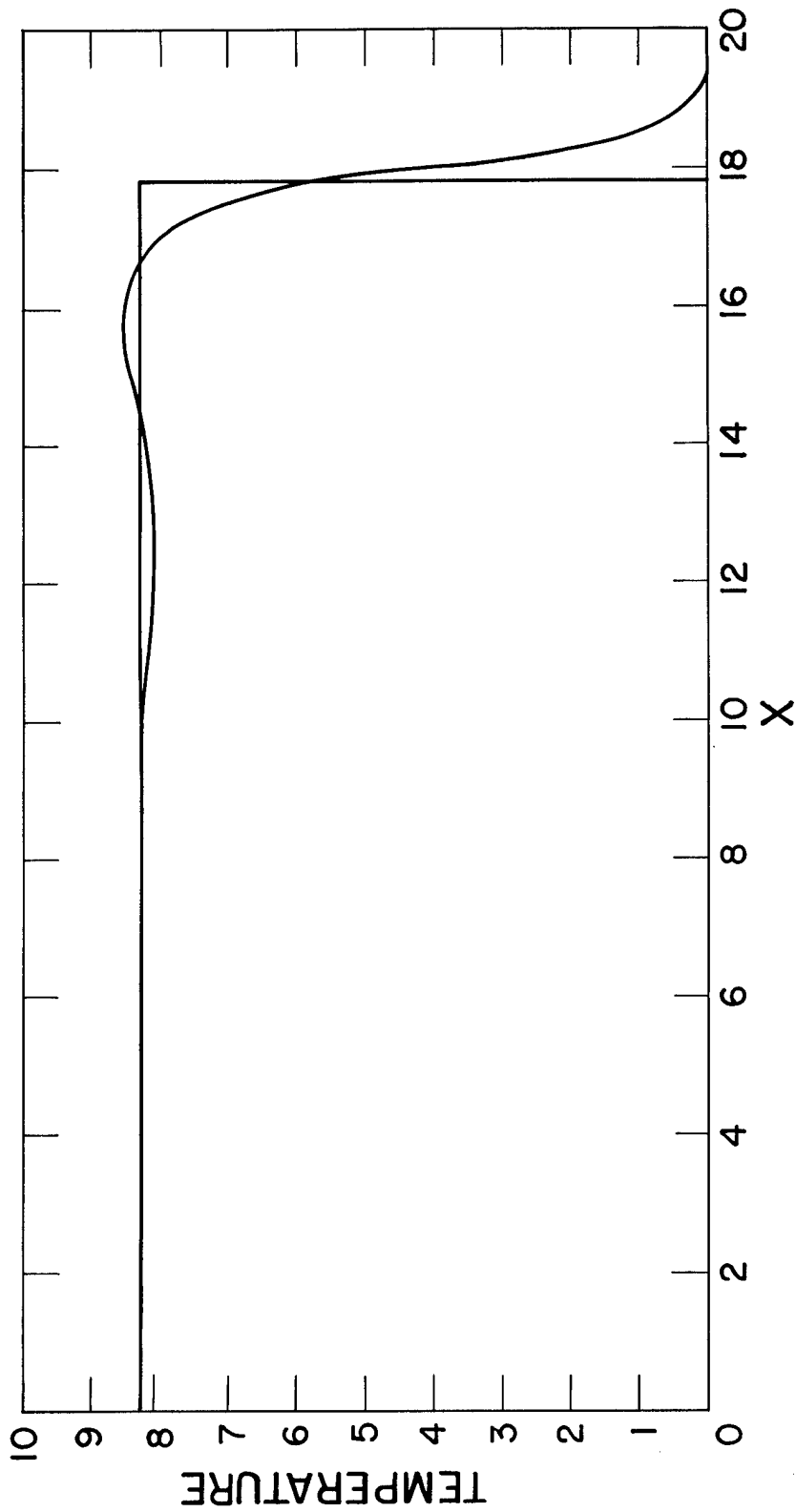
Fig. 1 Temperature profile for a steady-state shock. Straight lines form the theoretical profile.
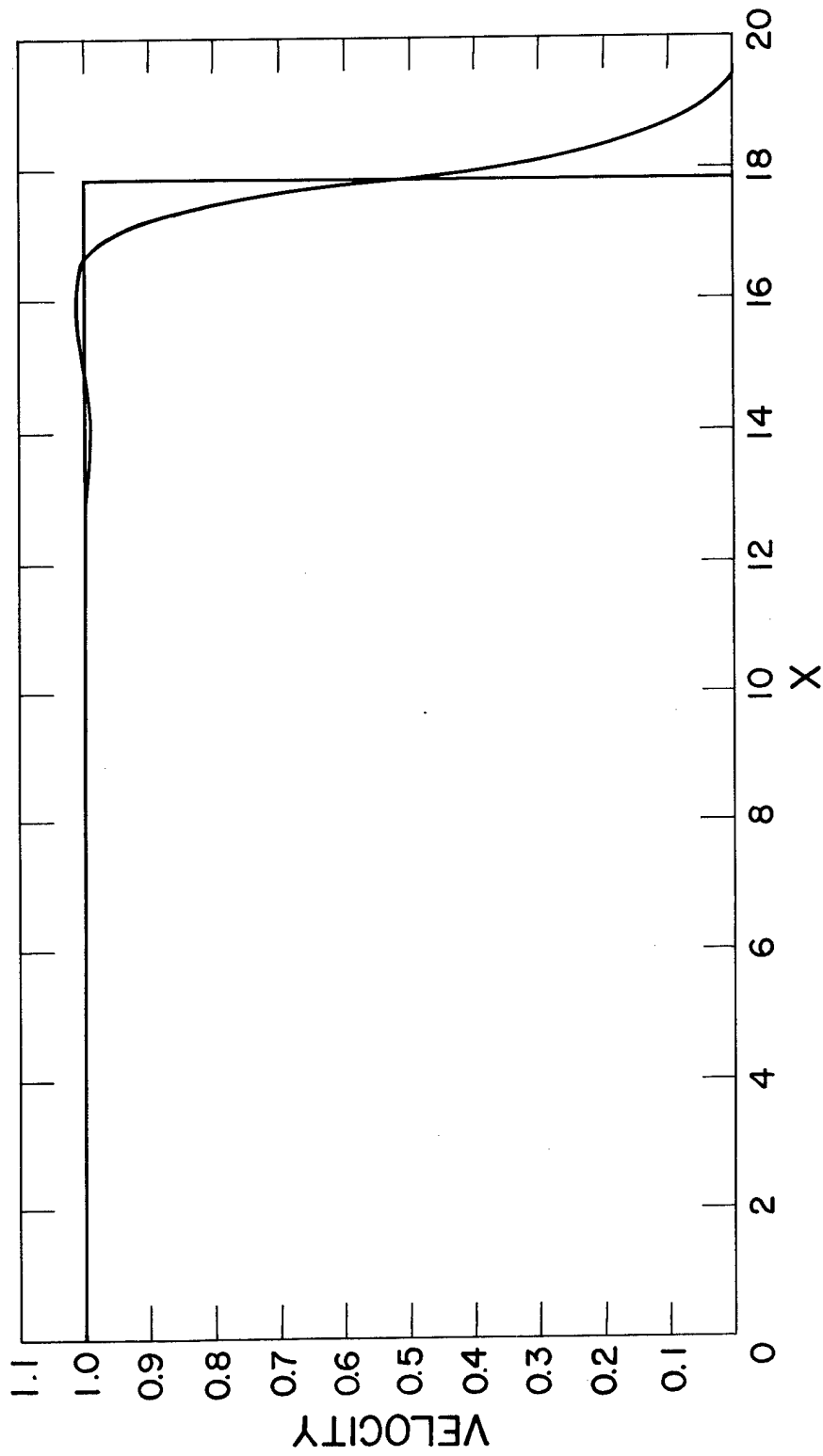
Fig. 2 Velocity profile for a steady-state shock. Straight lines form the theoretical profile.
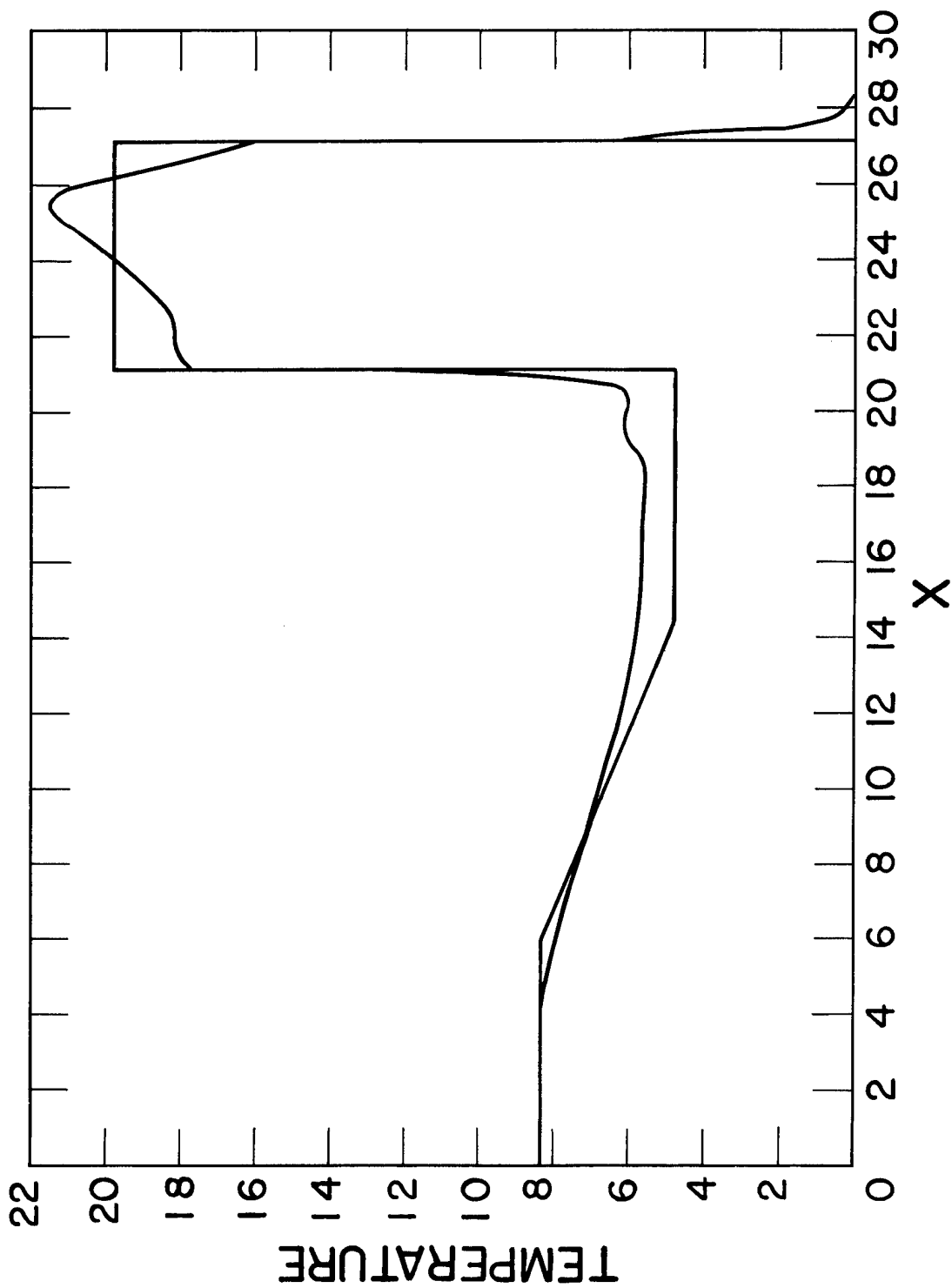
Fig. 3 Temperature profile for a shock having hit a density decrease. Straight lines form the theo-retical profile (approximate in the rarefaction wave zone).
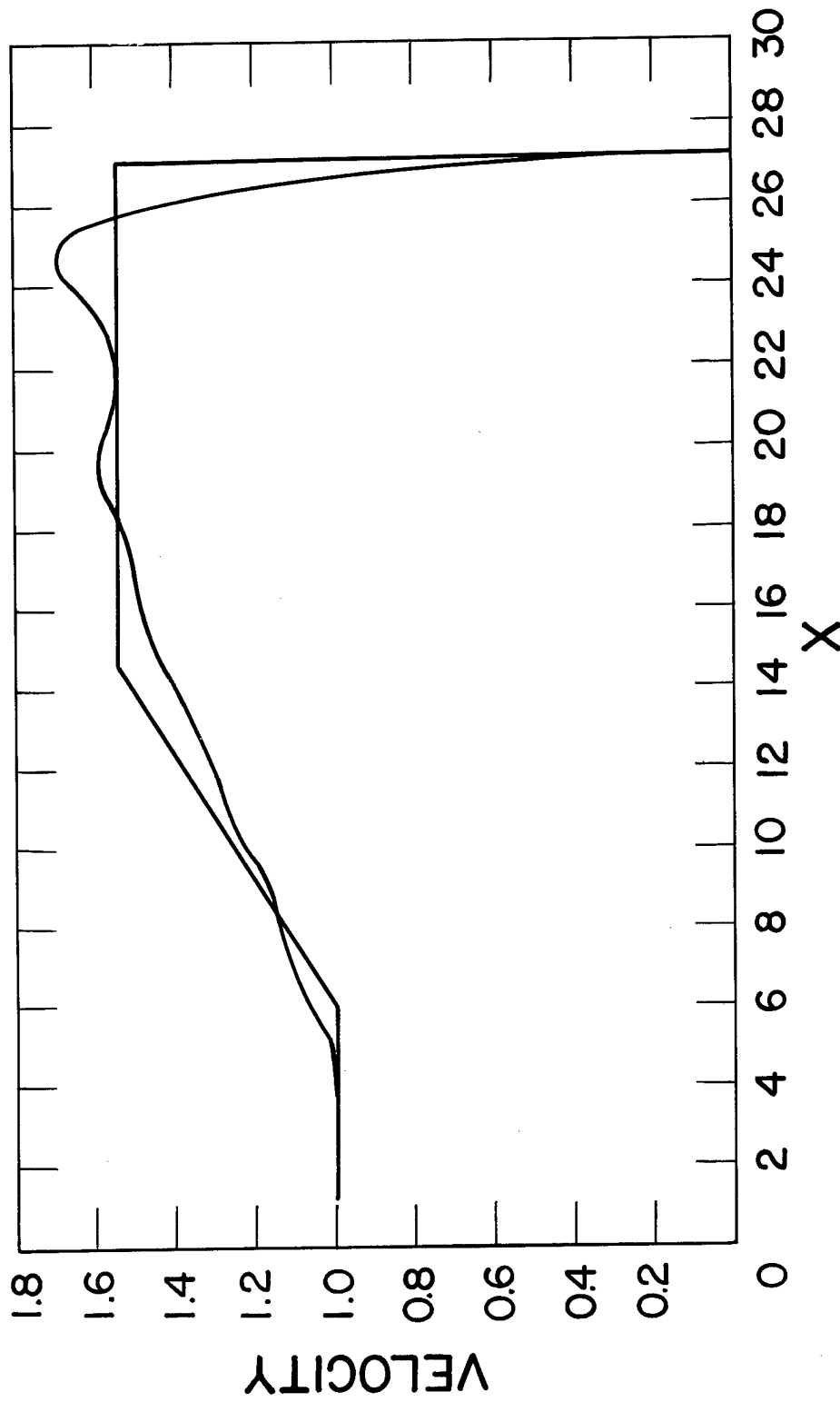
Fig. 4 Velocity profile for a shock having hit a density decrease. Straight lines form the theoretical profile.
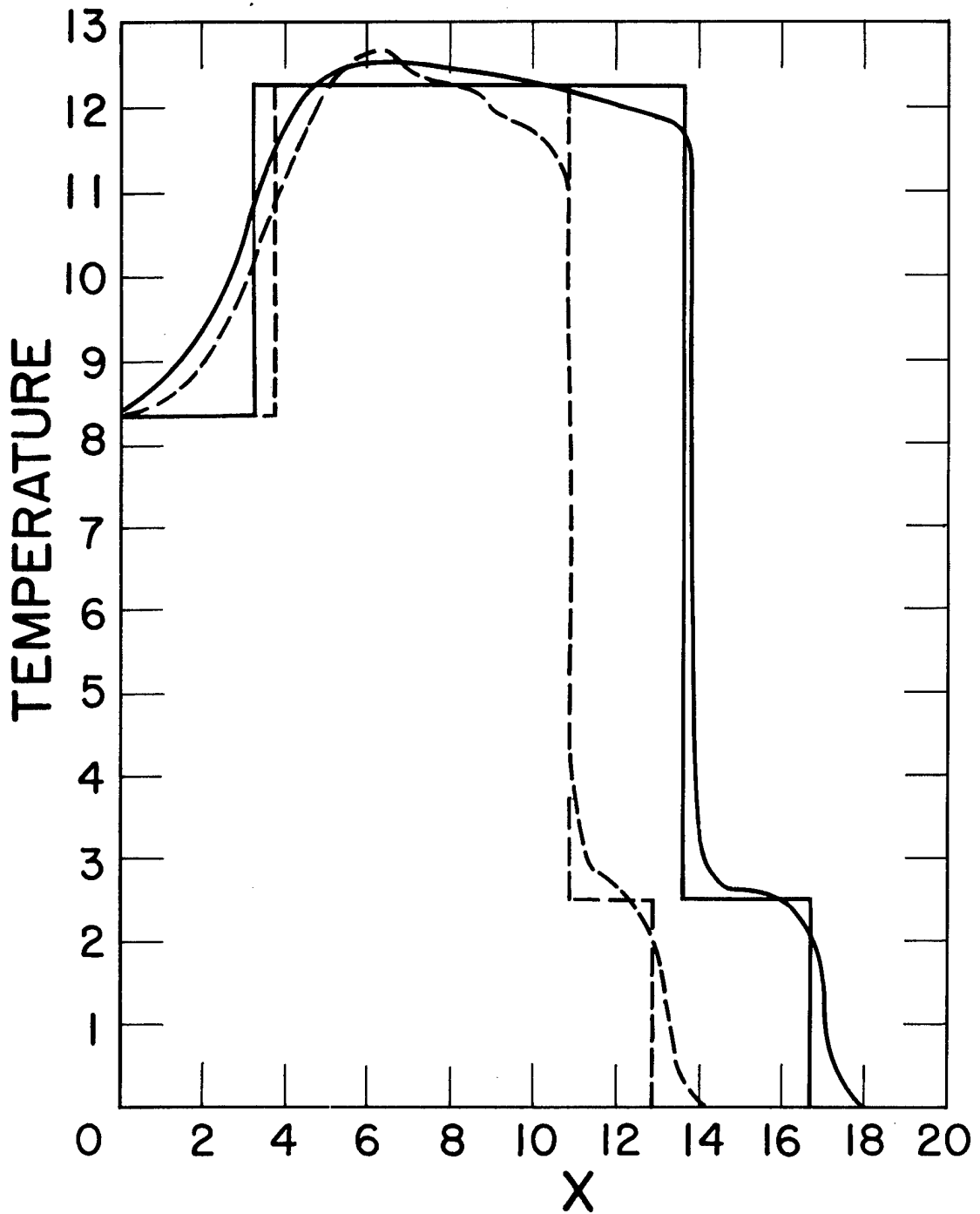
Fig. 5 Temperature profile for a shock having hit a density increase.
Straight lines form the theoretical profile. The two curves are at
different times.
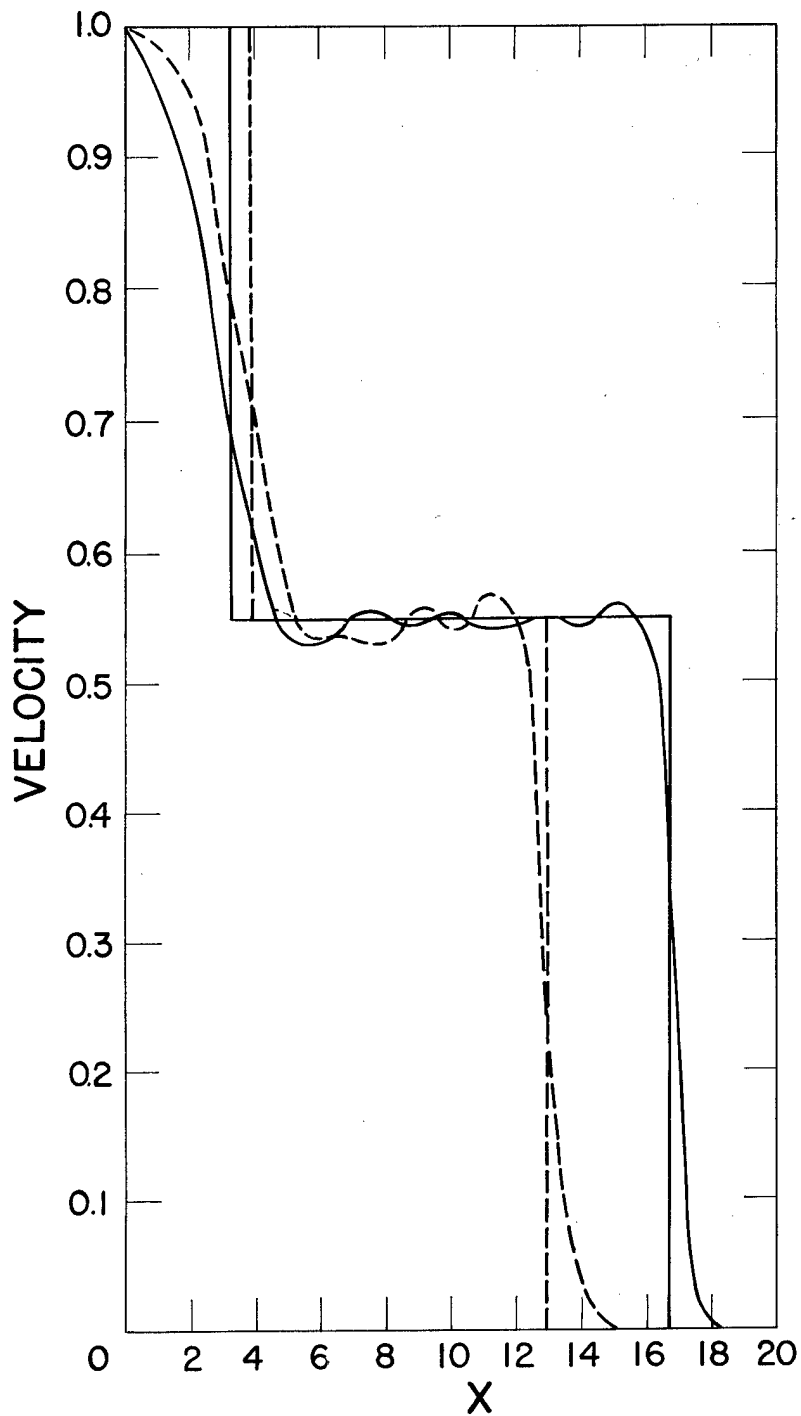
Fig. 6 Velocity profile for a shock having hit a density increase. Straight
lines form the theoretical profile. The two curves are at different
times.
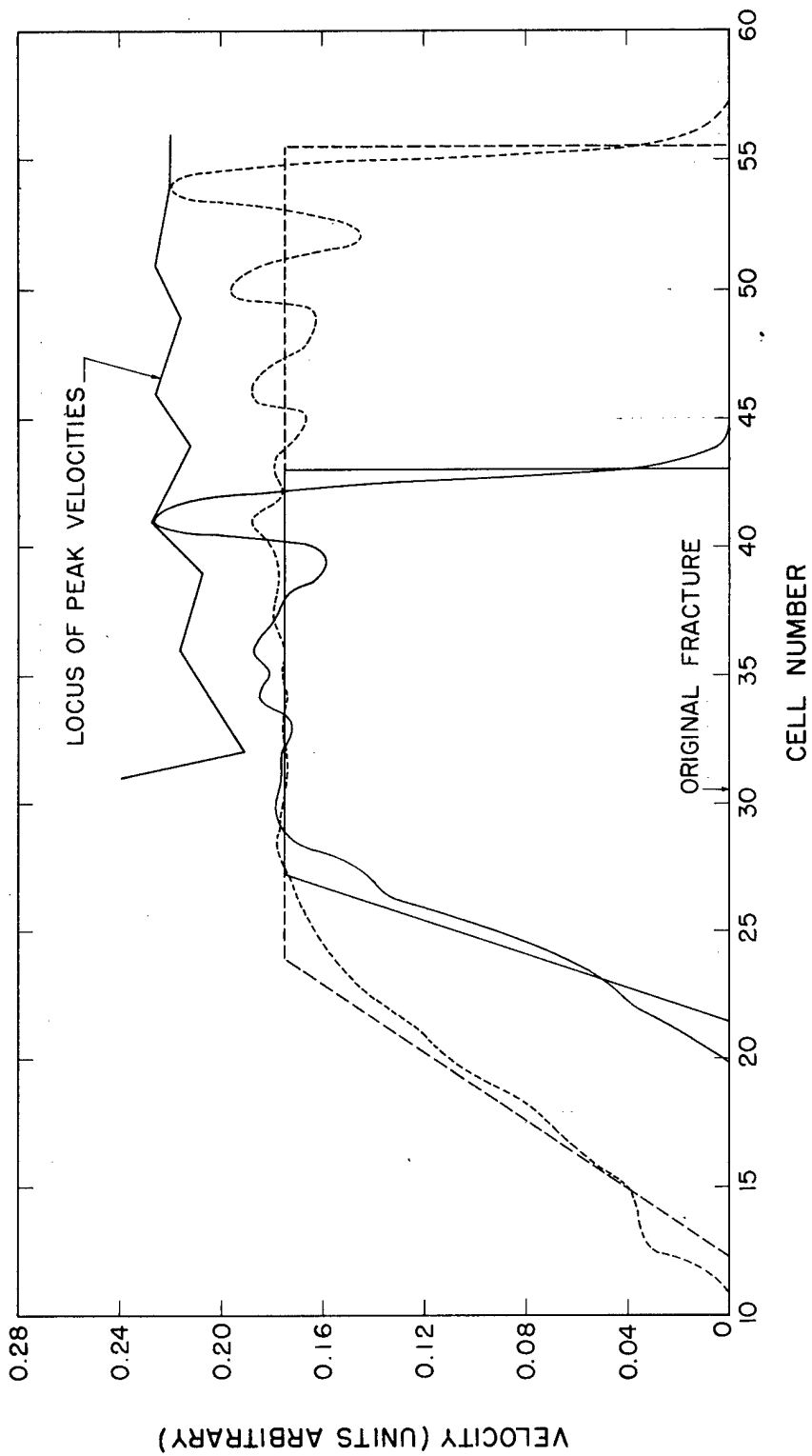
Fig. 7 Velocity profiles for shock tube after 250 and 500 machine cycles. Position and magnitude of peak velocity is shown for every 50 cycles. Straight lines show the theoretical profile.
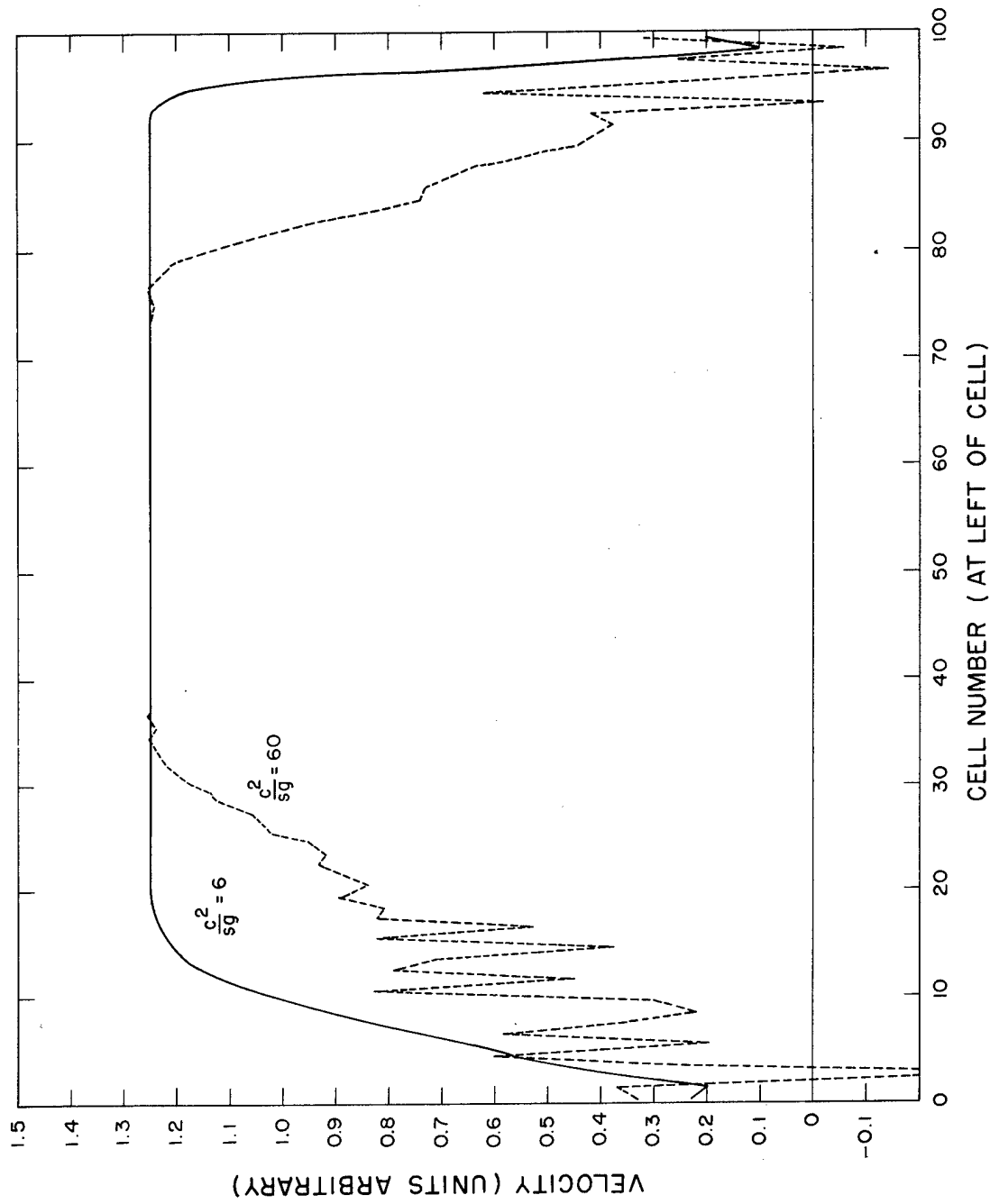
Fig. 8 Velocity profiles for one-dimensional gravity problem after 250 time cycles. Variations in c^2/sg result from changing the initial temperature. Each calculation had 8 particles per cell, initially.
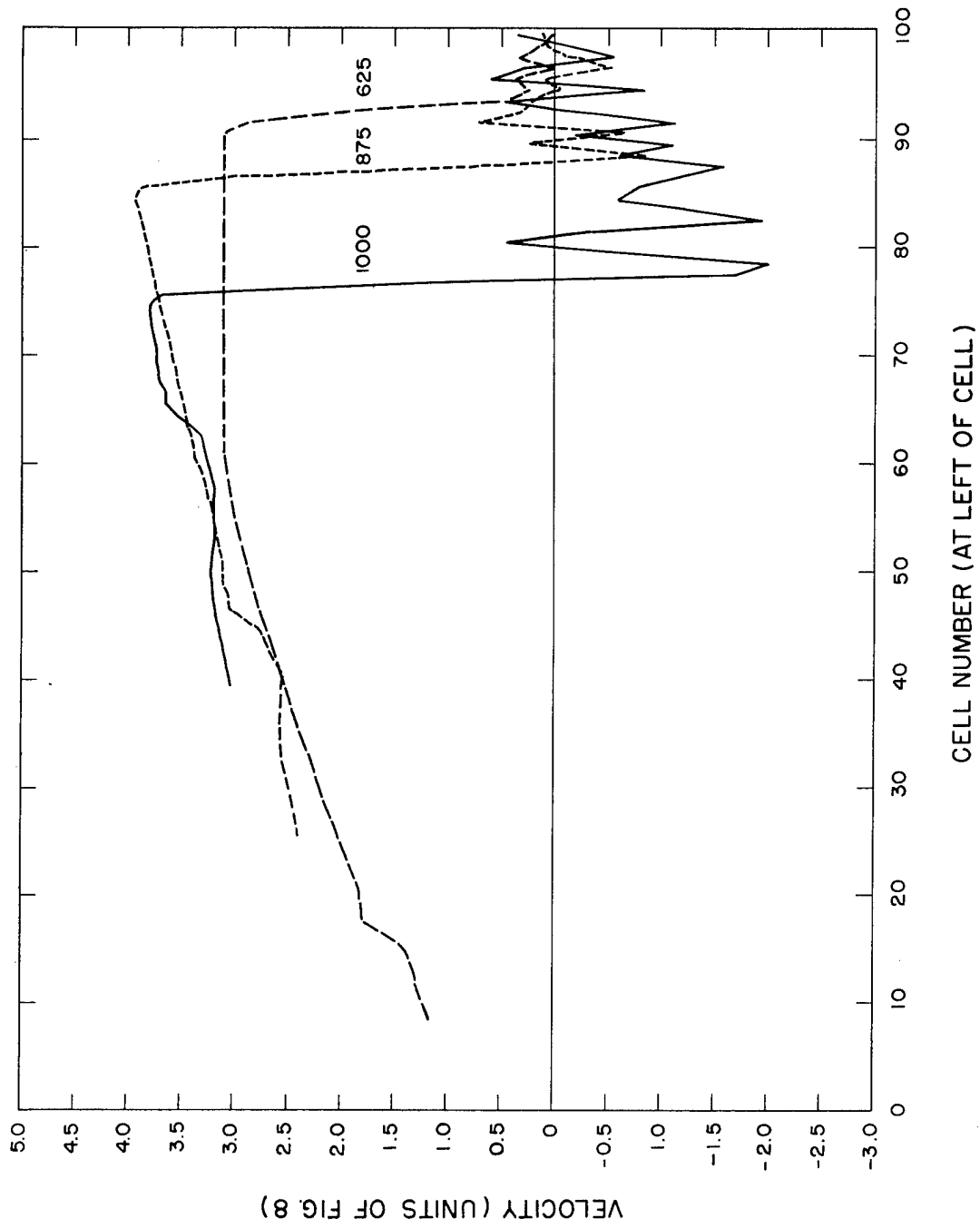
Fig. 9 Further development of the smoother curve of Fig. 8. Number of time cycles is shown for each curve.
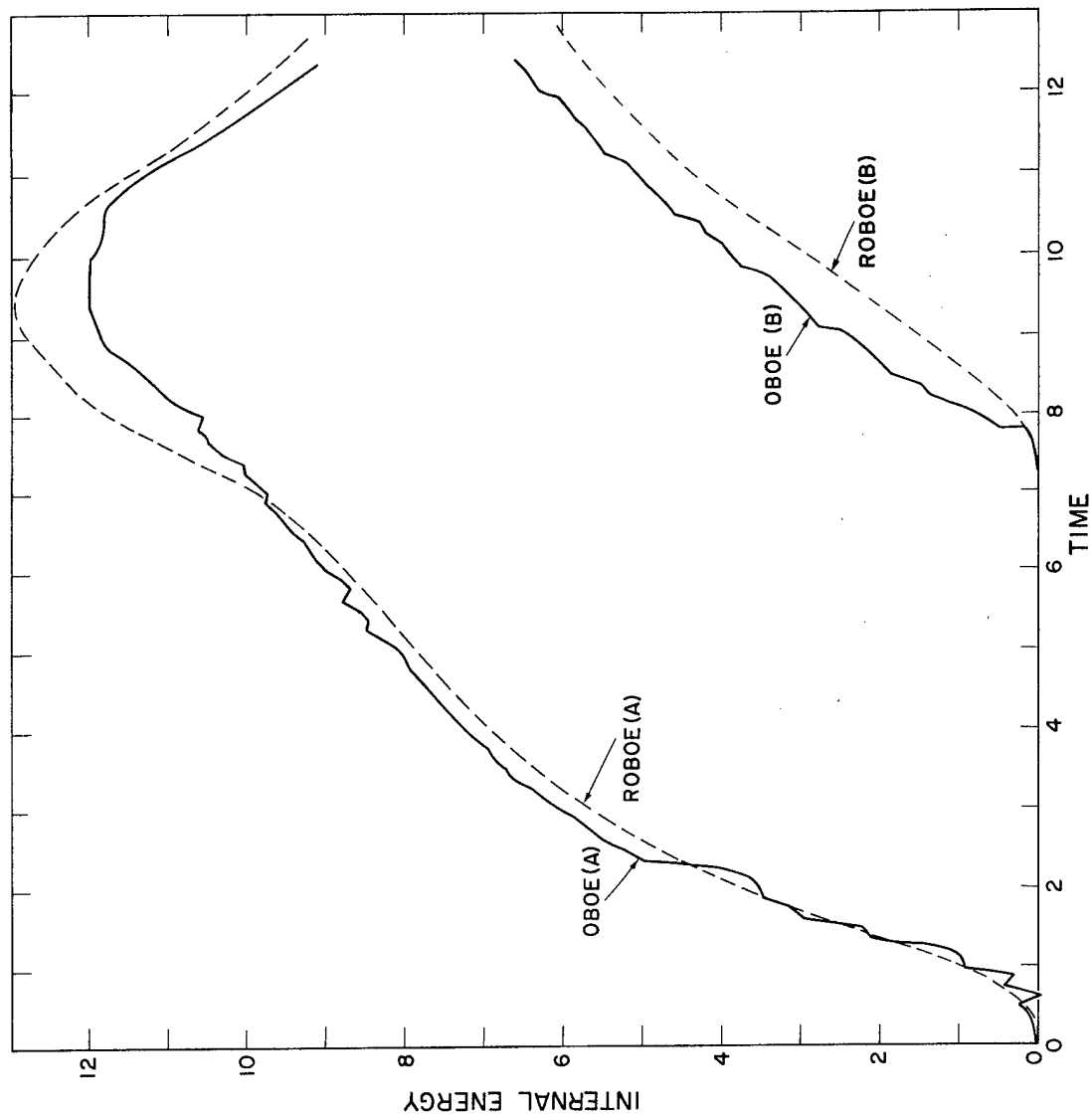
Fig. 10 Internal energy for gases A and B for the problems OBOE and ROBOE. The units are arbitrary.
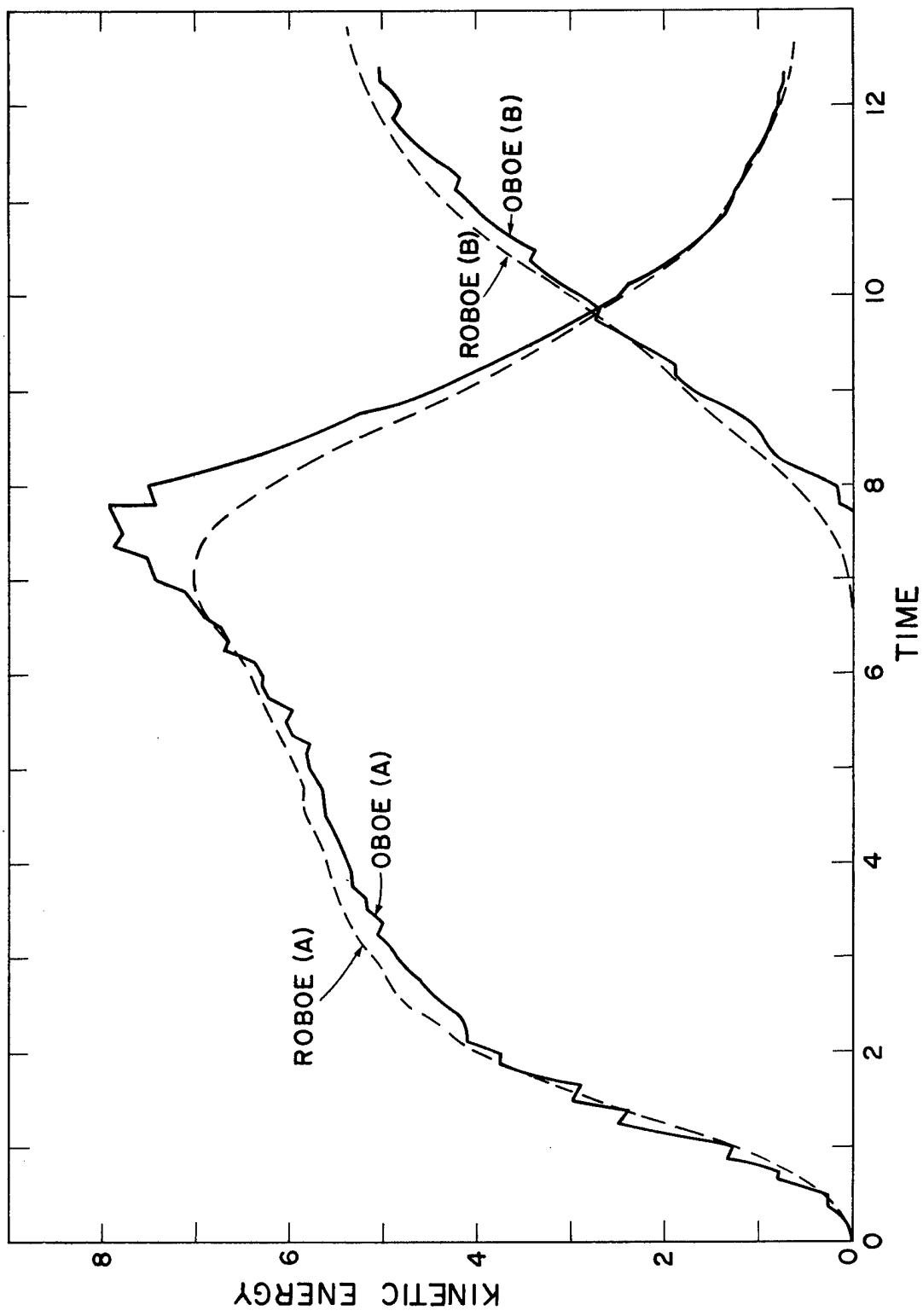
Fig. 11 Kinetic energy for gases A and B for the problems OBOE and ROBOE. The units are arbitrary.
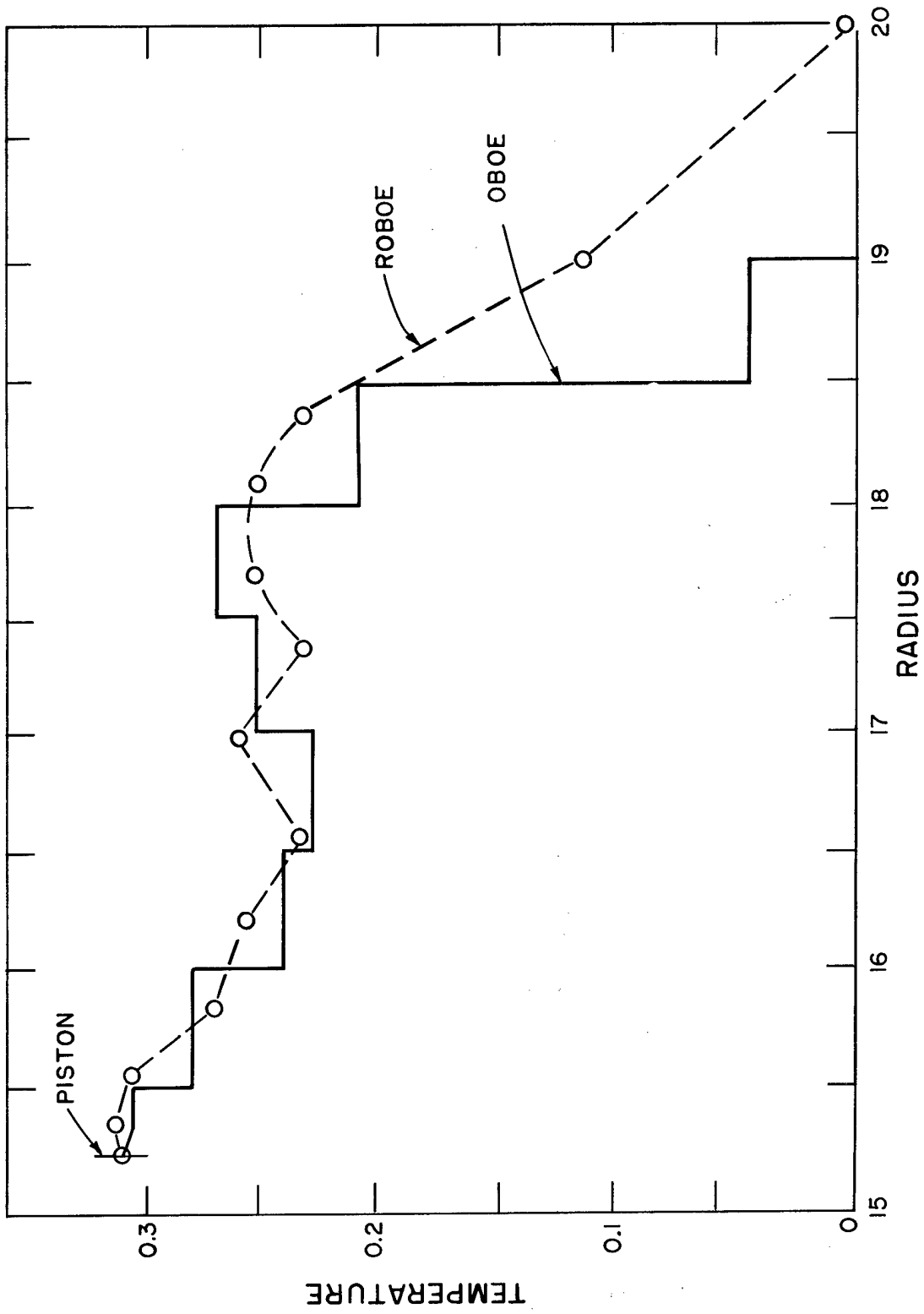
Fig. 12 Velocity profile in OBOE and ROBOE at time 6-1/2.
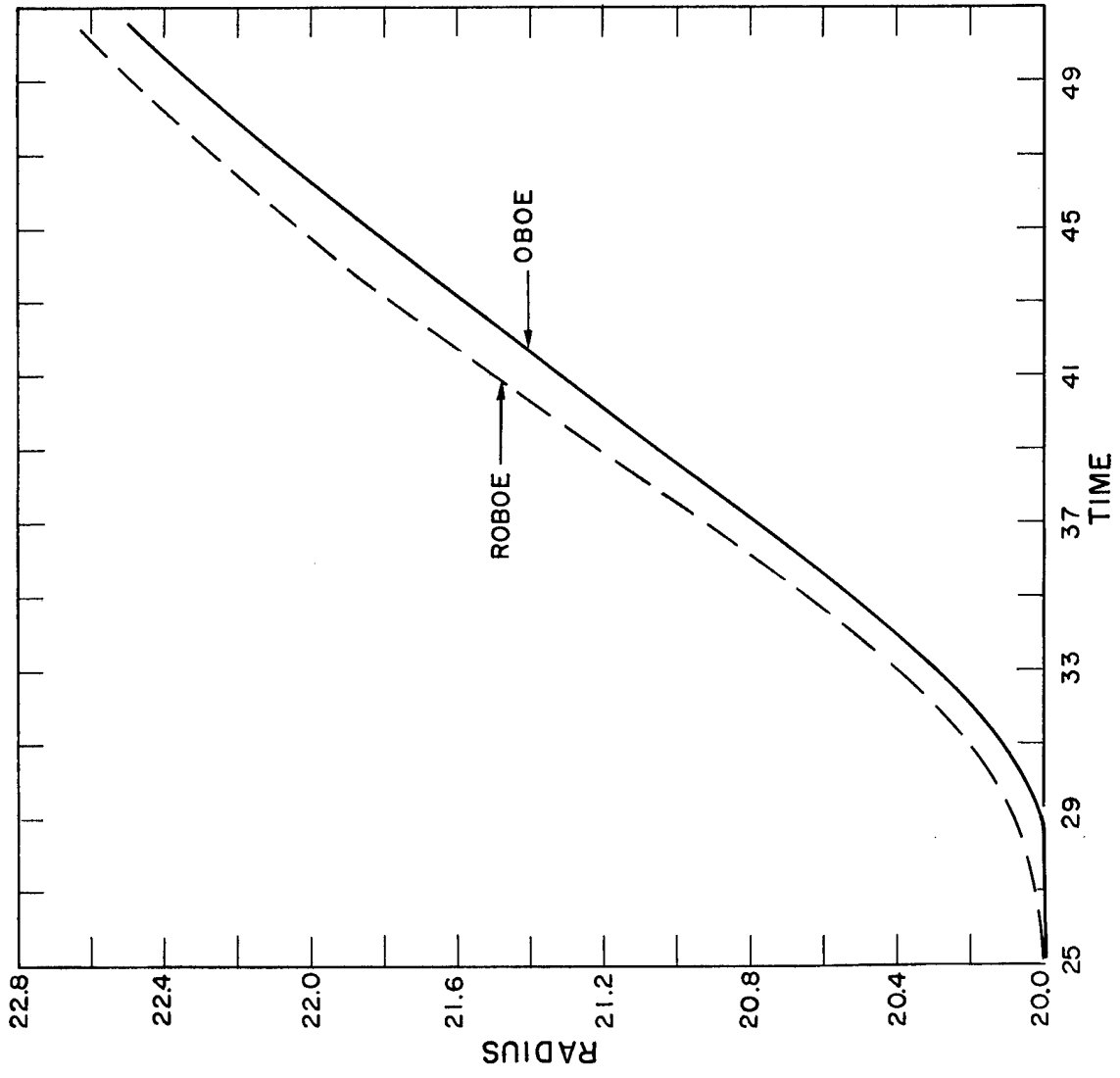
Fig. 13 Position of the A–B boundary as a function of time for the problems OBOE and ROBOE.
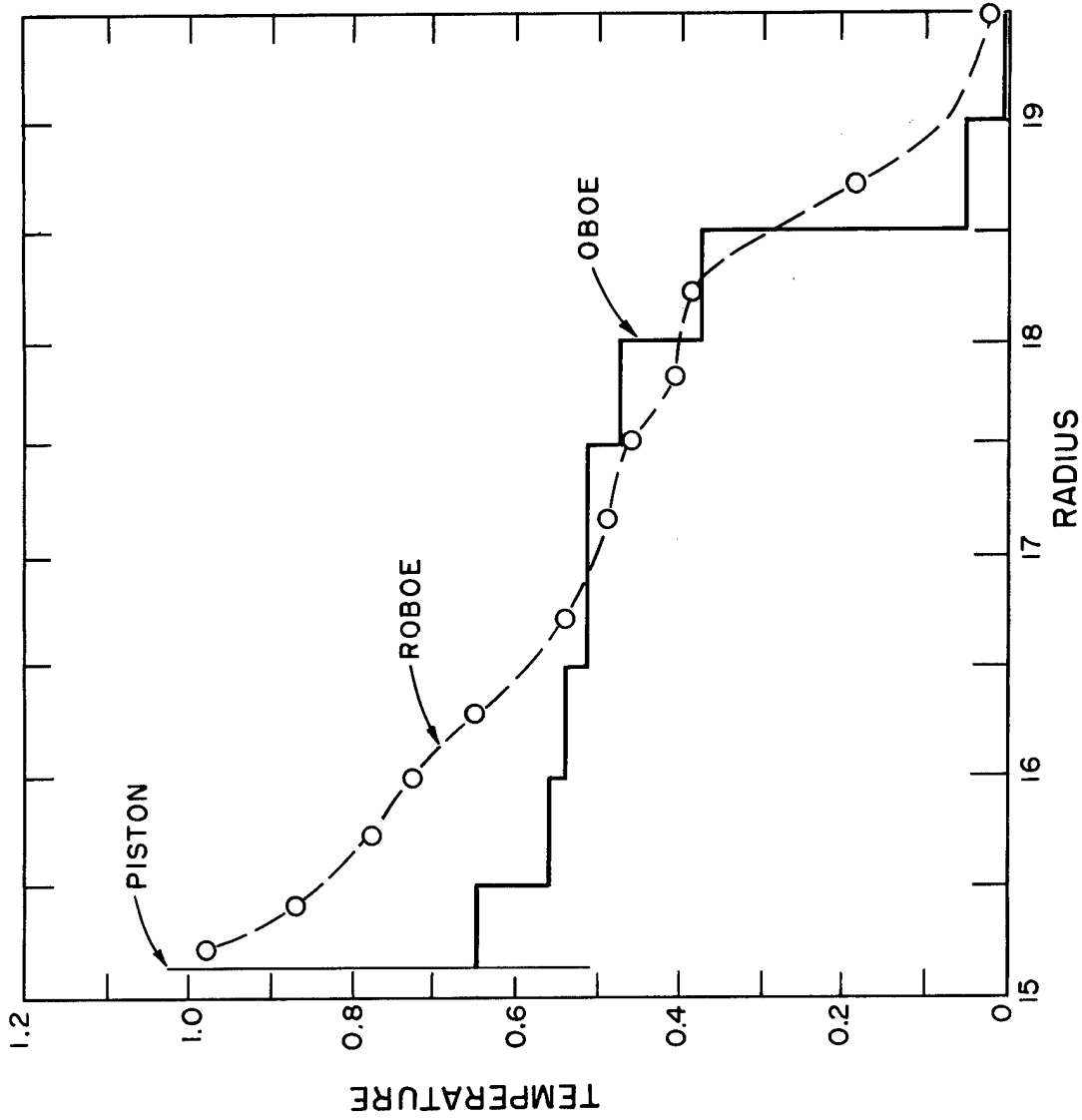
Fig. 14   Temperature profile in OBOE and ROBOE at time 6-1/2.   The temperature units are arbitrary.
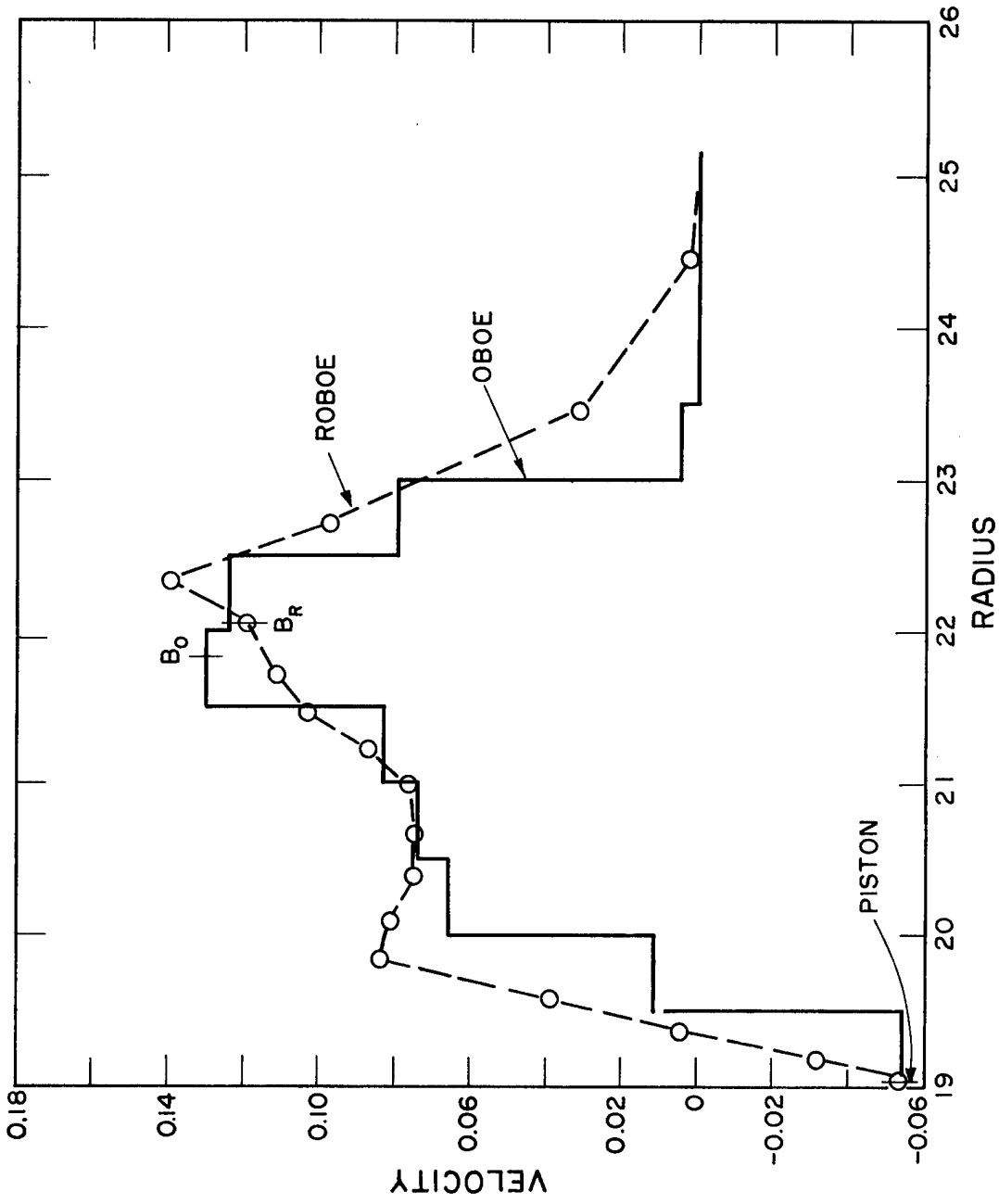
Fig. 15 Velocity profile in OBOE and ROBOE at time t = 11-1/4. B_O and B_R are the A-B boundary positions.
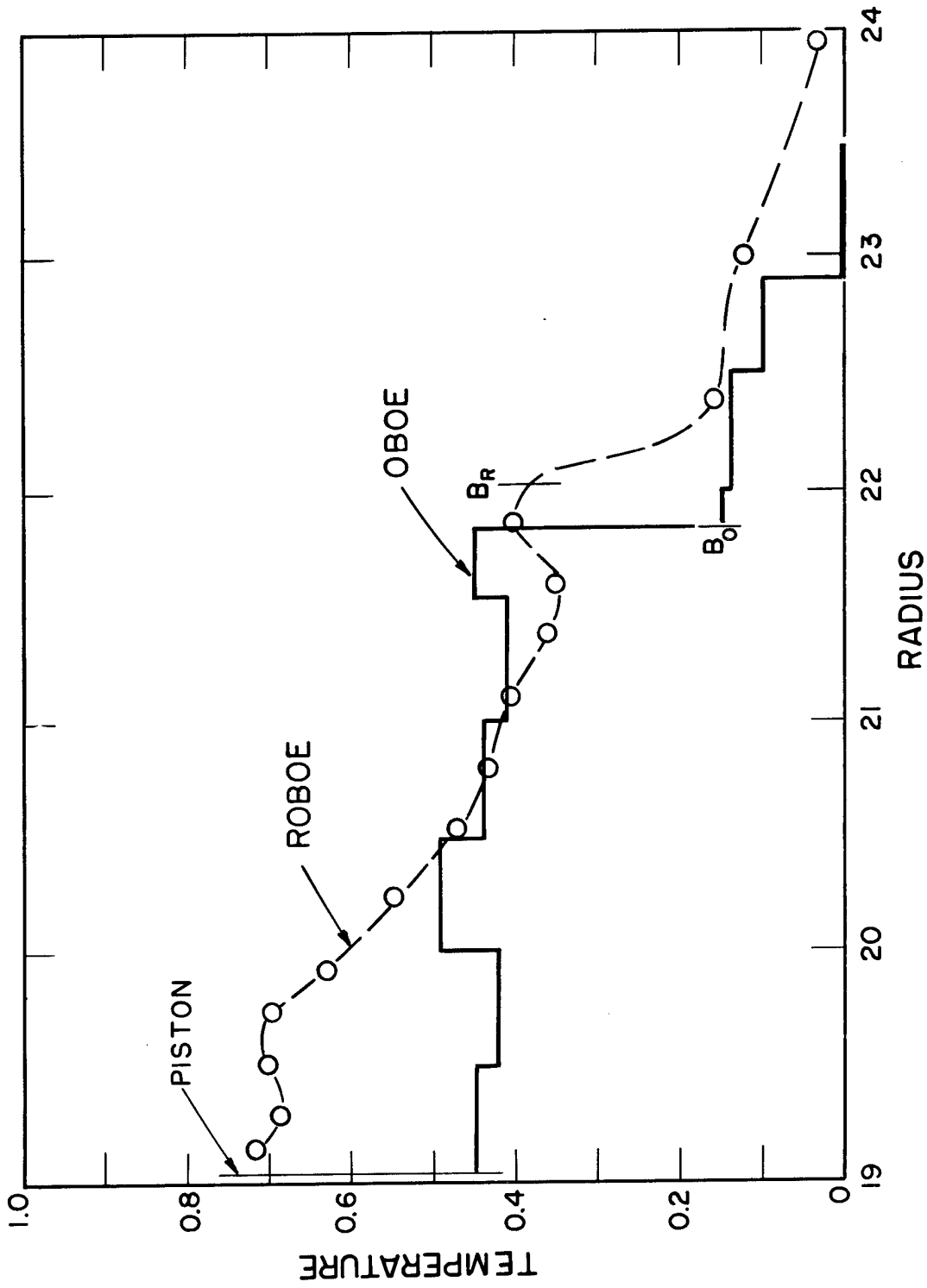
Fig. 16 Temperature profile in OBOE and ROBOE at time 11-1/4. The temperature units are arbitrary. B_O and B_R are the boundary positions.
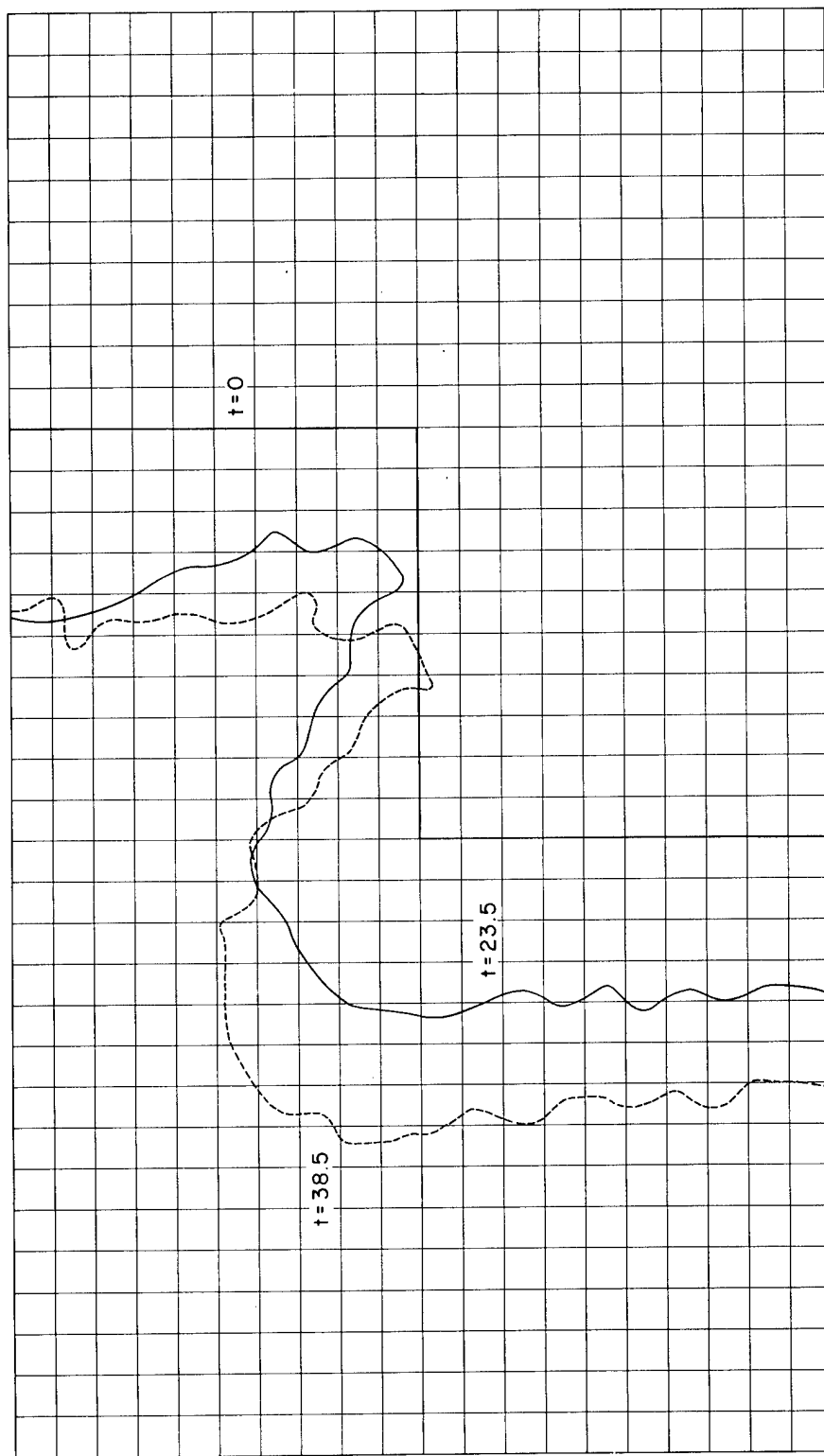
Fig. 17 Interface positions between two gases at various times.
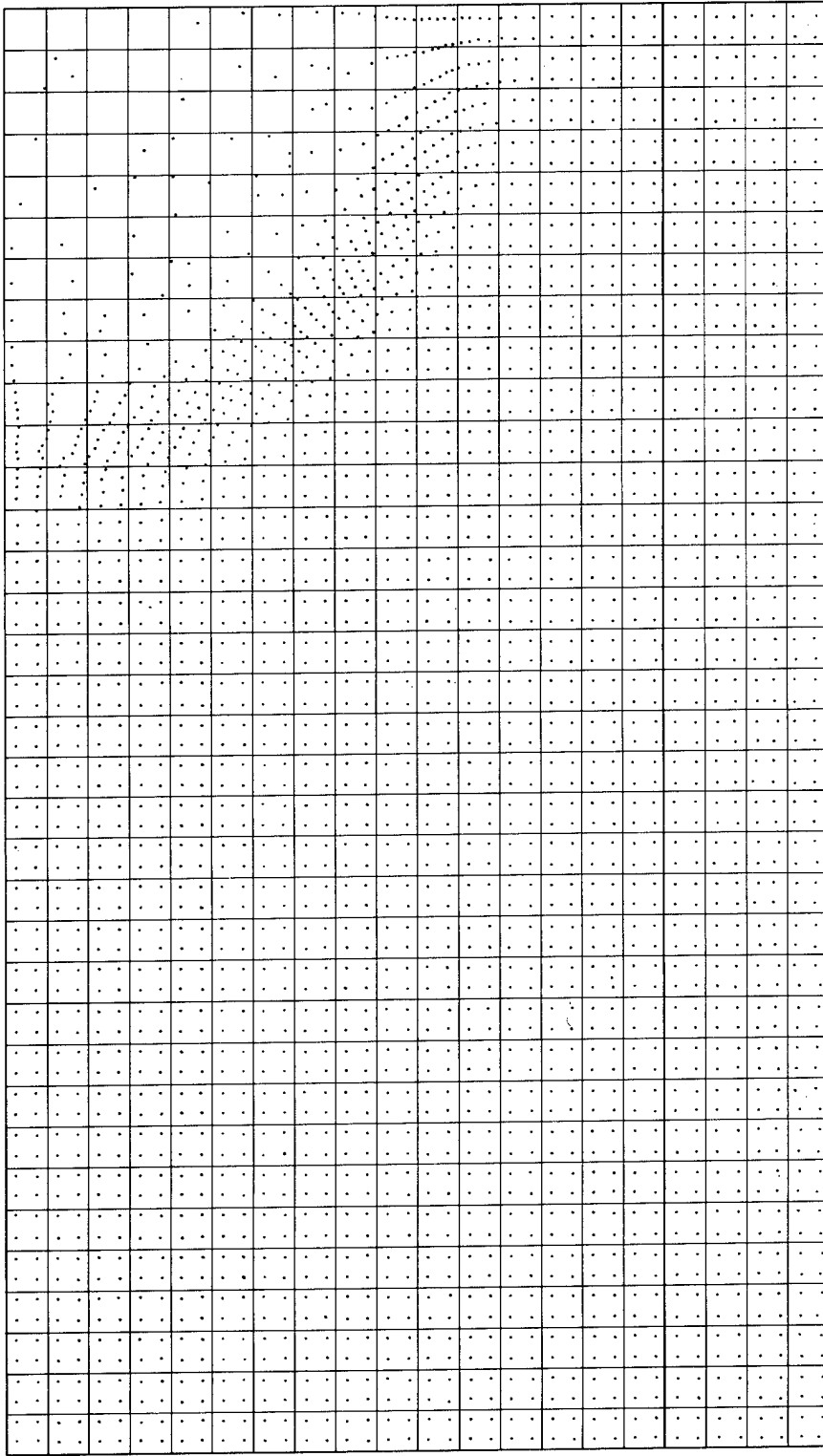
Fig. 18 Particle configuration in cylindrical shock problem at t = 4.8.
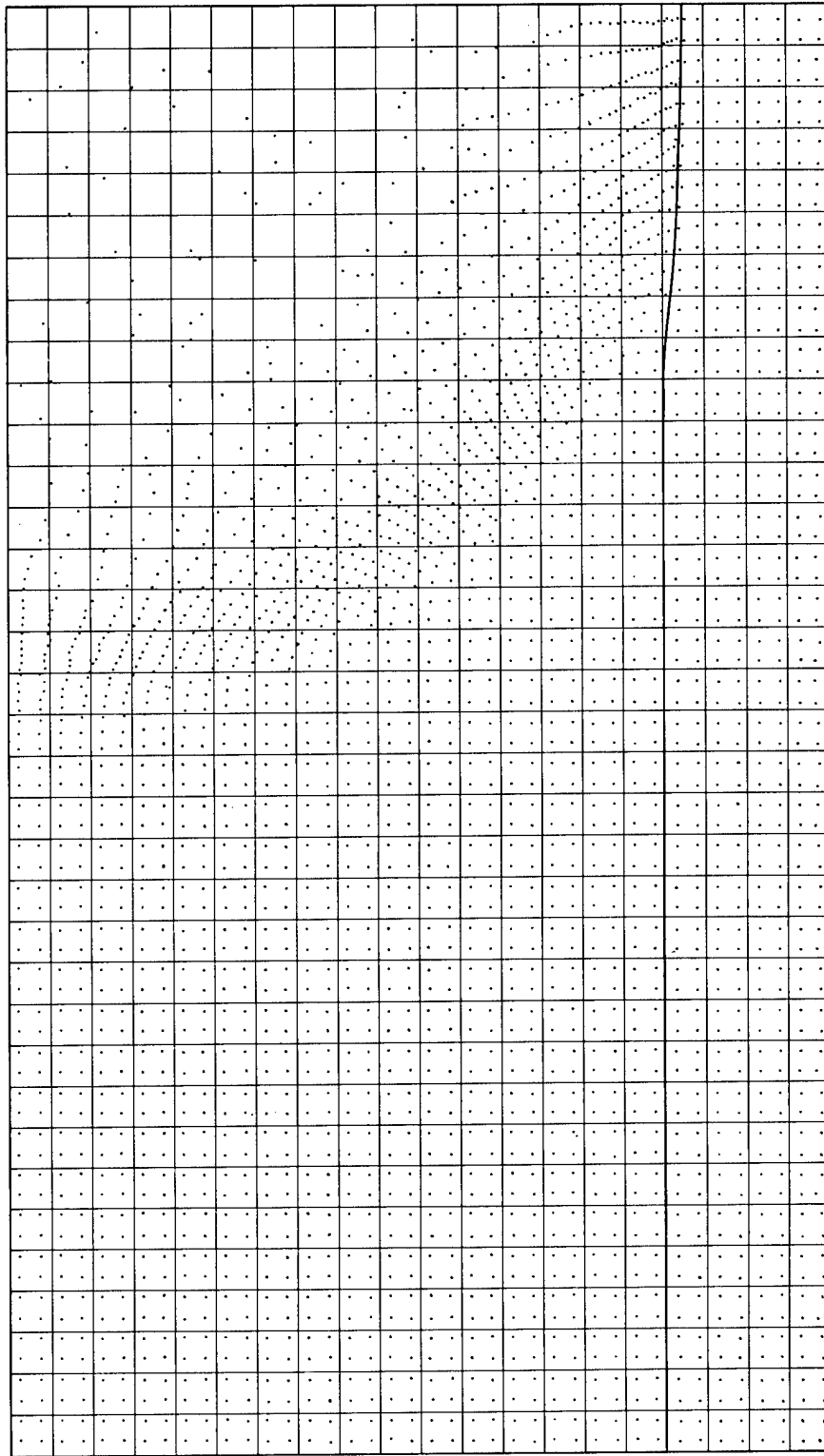
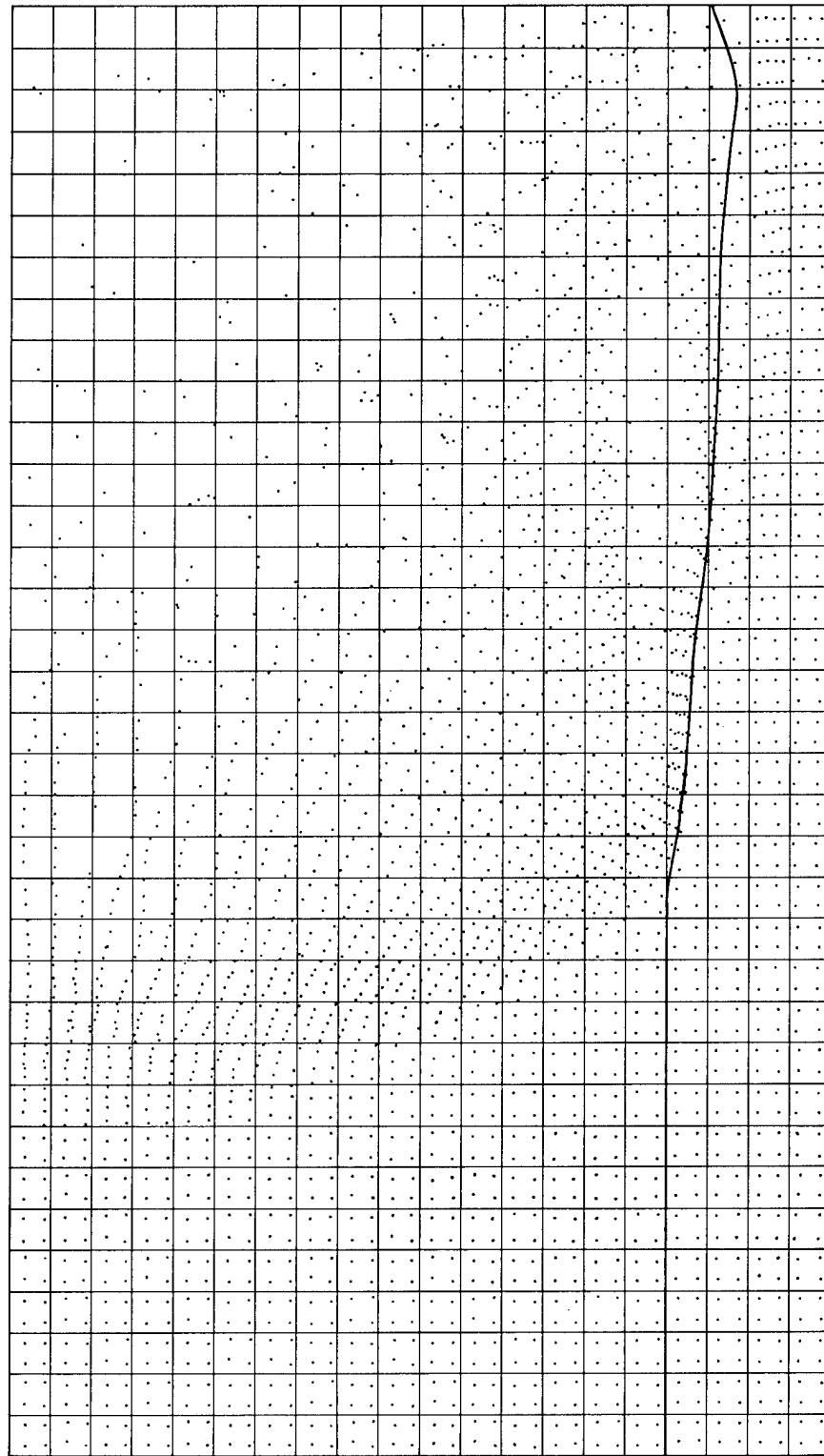Fig. 19 Particle configuration in cylindrical shock problem at t = 9.8.
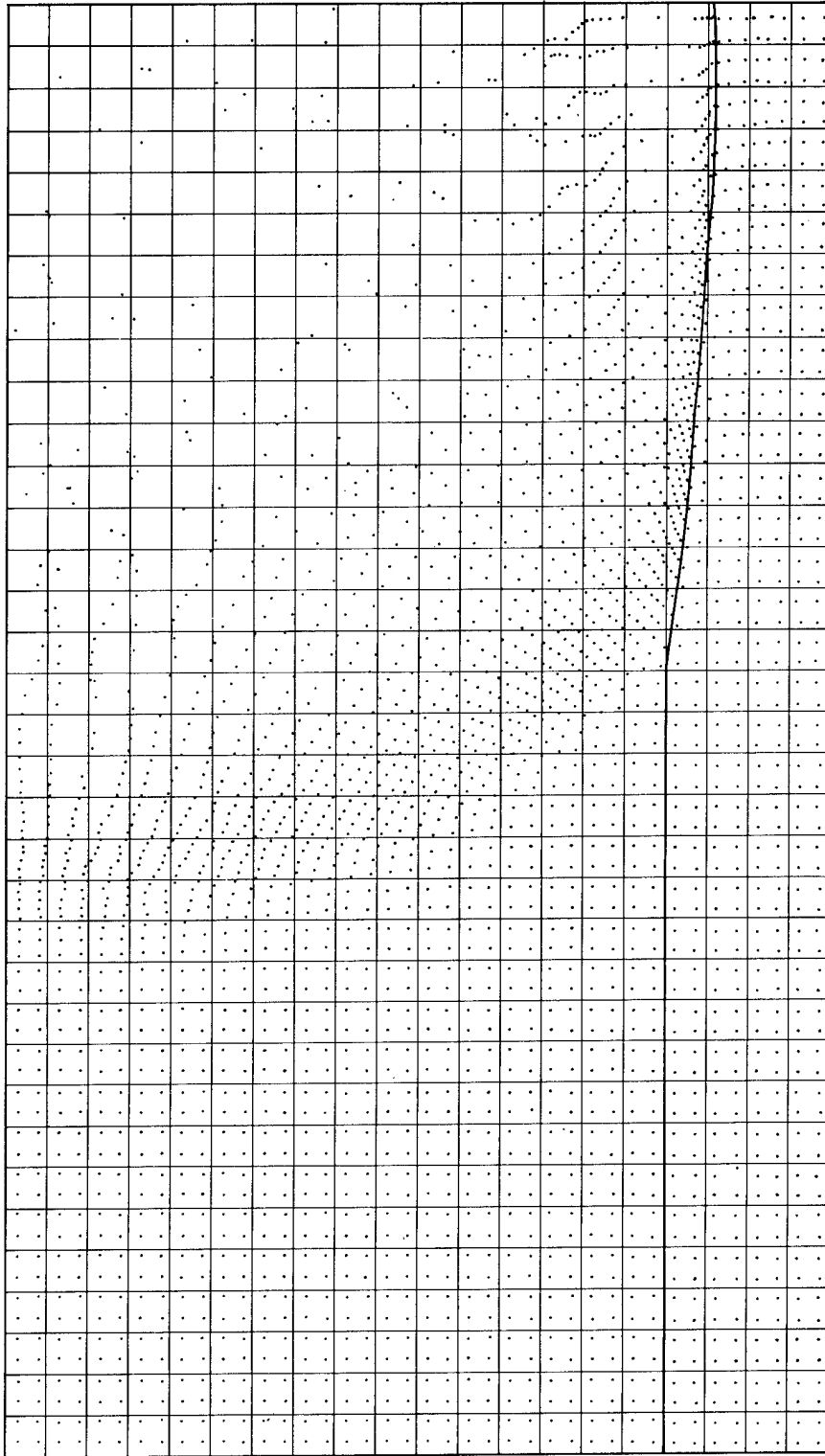
Fig. 20 Particle configuration in cylindrical shock problem at 6 = 16.0

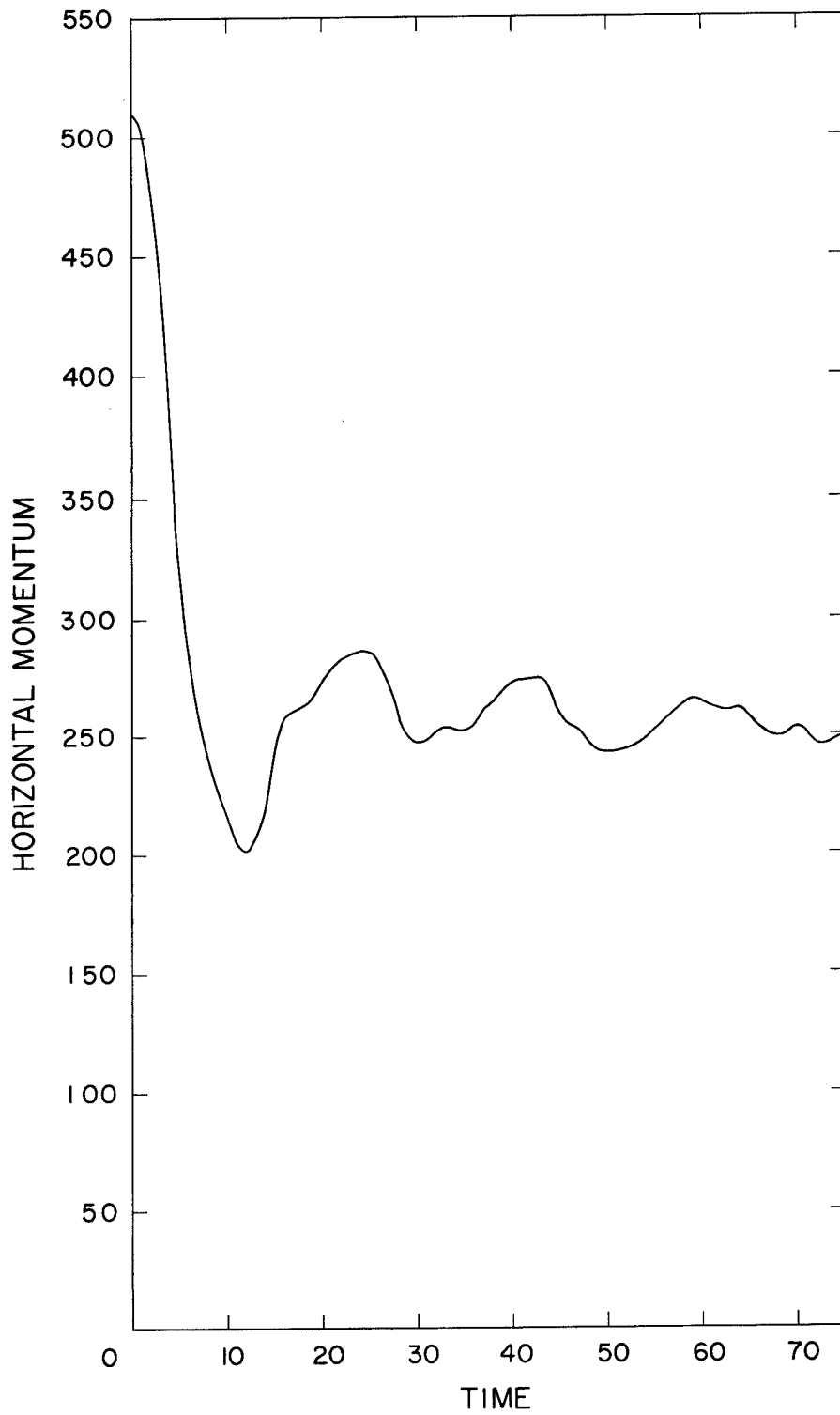Fig. 21 Particle configuration in cylindrical shock problem at t = 22.0.
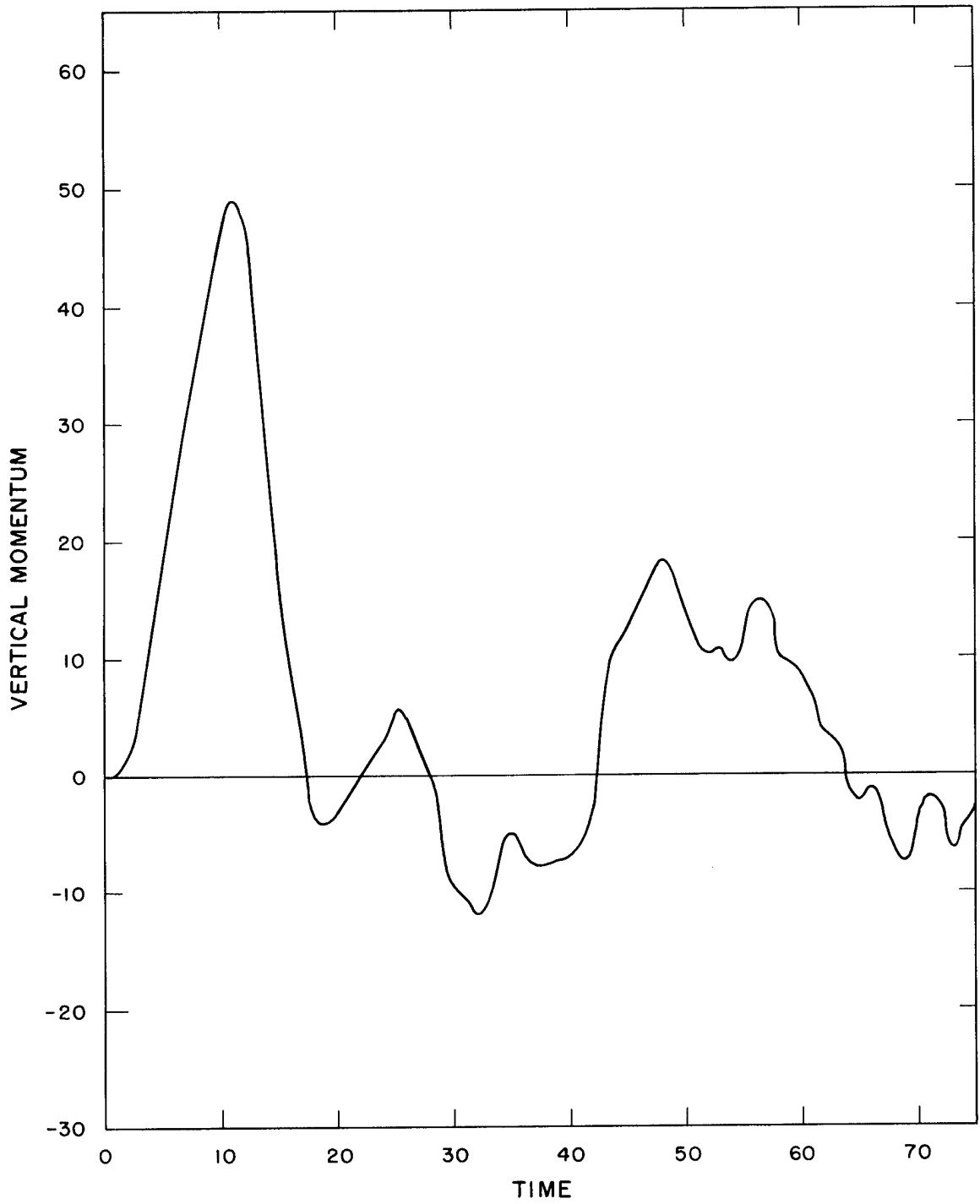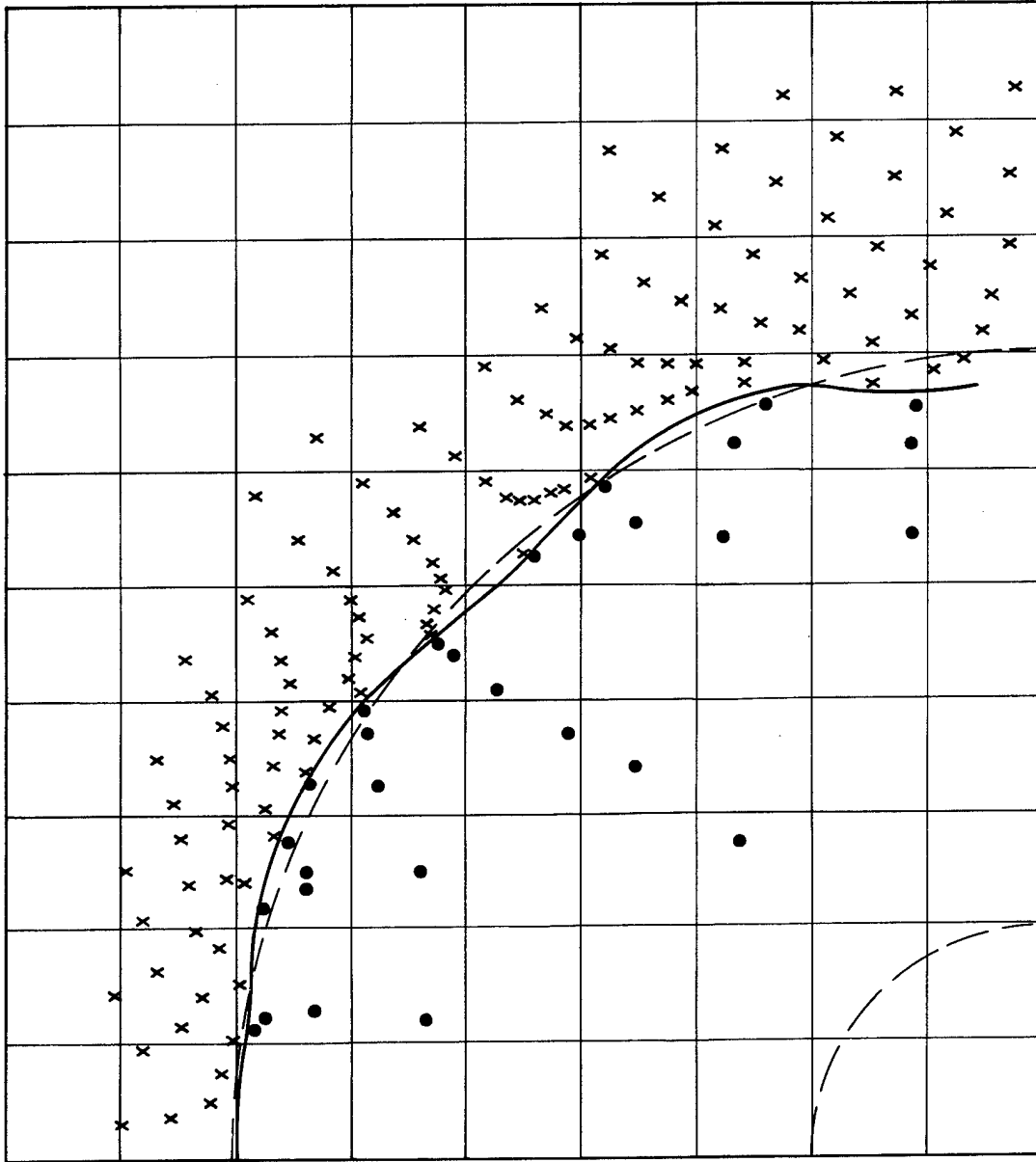
Fig. 22 Horizontal momentum in KAREN problem.

Fig. 23 Vertical momentum in KAREN problem.

AXIS

Fig. 24   Particle configuration for sphericity test problem at a late time.